Remediation of mercury contaminated soil, water, and air: A review of emerging materials and innovative technologies

Liuwei Wang[a], Deyi Hou[a,*], Yining Cao[a], Yong Sik Ok[b], Filip M.G. Tack[c], Jörg Rinklebe[d,e], David O'Connor[a]

[a] School of Environment, Tsinghua University, Beijing 100084, China
[b] Korea Biochar Research Center & Division of Environmental Science and Ecological Engineering, Korea University, Seoul 02841, Republic of Korea
[c] Department of Green Chemistry and Technology, Ghent University, Coupure Links 653, 9000 Ghent, Belgium
[d] University of Wuppertal, School of Architecture and Civil Engineering, Institute of Foundation Engineering, Water- and Waste-Management, Laboratory of Soil- and Groundwater-Management, Pauluskirchstraße 7, Wuppertal 42285, Germany
[e] Department of Environment, Energy and Geoinformatics, Sejong University, 98 Gunja-Dong, Seoul, Republic of Korea

ARTICLE INFO

ABSTRACT

Mercury contamination in soil, water and air is associated with potential toxicity to humans and ecosystems. Industrial activities such as coal combustion have led to increased mercury (Hg) concentrations in different environmental media. This review critically evaluates recent developments in technological approaches for the remediation of Hg contaminated soil, water and air, with a focus on emerging materials and innovative technologies. Extensive research on various nanomaterials, such as carbon nanotubes (CNTs), nanosheets and magnetic nanocomposites, for mercury removal are investigated. This paper also examines other emerging materials and their characteristics, including graphene, biochar, metal organic frameworks (MOFs), covalent organic frameworks (COFs), layered double hydroxides (LDHs) as well as other materials such as clay minerals and manganese oxides. Based on approaches including adsorption/desorption, oxidation/reduction and stabilization/containment, the performances of innovative technologies with the aid of these materials were examined. In addition, technologies involving organisms, such as phytoremediation, algae-based mercury removal, microbial reduction and constructed wetlands, were also reviewed, and the role of organisms, especially microorganisms, in these techniques are illustrated.

1. Introduction

Mercury (Hg) is a toxic heavy metal that has been regarded as one of the "ten leading chemicals of concern" (WHO, 2017). According to the United Nations Environment Programme (UNEP) report (UNEP, 2018), it is estimated that global mercury emissions to air from anthropogenic sources in 2015 were about 2220 tons. Among the anthropogenic sources, stationary combustion of fossil fuels accounts for 24% of the estimated emissions, primarily from coal-burning (21%) (UNEP, 2018). Other anthropogenic sources include cement production (Wang et al., 2016b), iron and steel production (Wang et al., 2016a), nonferrous metal smelting (Wu et al., 2017b), gold production (Wu et al., 2018b), chlor-alkali industry (Busto et al., 2011; Busto et al., 2013; Kakareka and Kukharchyk, 2012), waste disposal (Pehnec et al., 2010) as well as direct production of mercury. Mercury contamination is of significant concern worldwide owing to its toxic effect on human health (Beckers and Rinklebe, 2017). Among the forms of inorganic mercury, the mercuric cation, Hg^{2+}, has proven to be a predominant toxic agent that can cause damage to kidney and lung (Clarkson and Magos, 2006). Once transformed into its organomercuric forms such as methylmercury (MeHg), Hg acts as a potent neurotoxin which impairs brain function. Apart from the high toxicity of this form of mercury, it has raised particular concern for its capability to biomagnify up the food chain (He et al., 2015; O'Connor et al., 2019; Selin, 2009).

Once emitted to the atmosphere, Hg can be transported and thoroughly mixed in its elemental form [Hg(0)]. The major sink of elemental mercury is deposition to soil or water bodies after oxidation to divalent mercury [Hg(II)] (Fig. 1) (O'Connor et al., 2019; Selin, 2009). Aside from deposition, point sources of mercury contamination are the predominant cause of Hg pollution in soil and water. Like other heavy metals, mercury cannot be degraded in ecosystems, and therefore remediation should be based on removal or immobilization processes
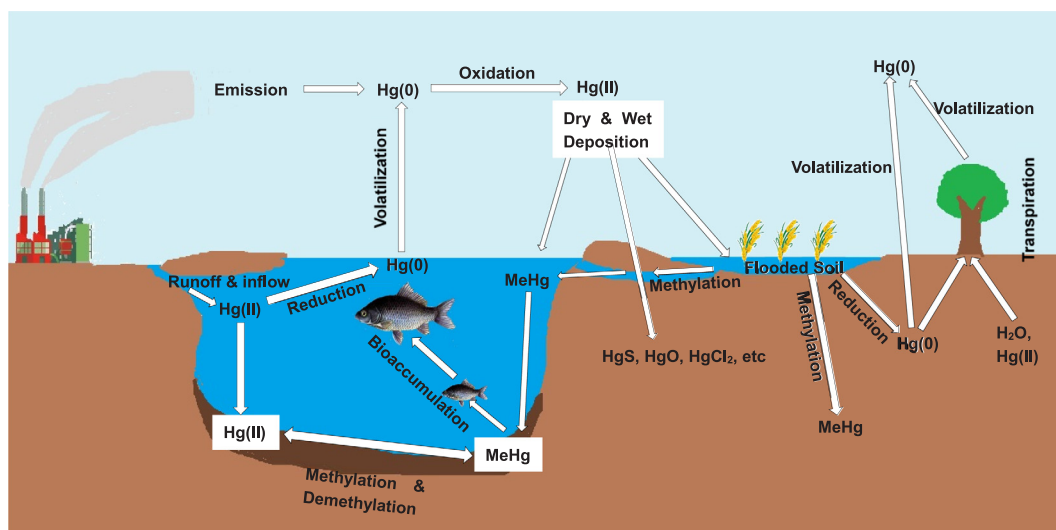
Fig. 1. Inter-phase transfer and transport of mercury in soil, water and air. Acronyms: Hg(0), elemental mercury; Hg(II), divalent mercury; MeHg, methylmercury.
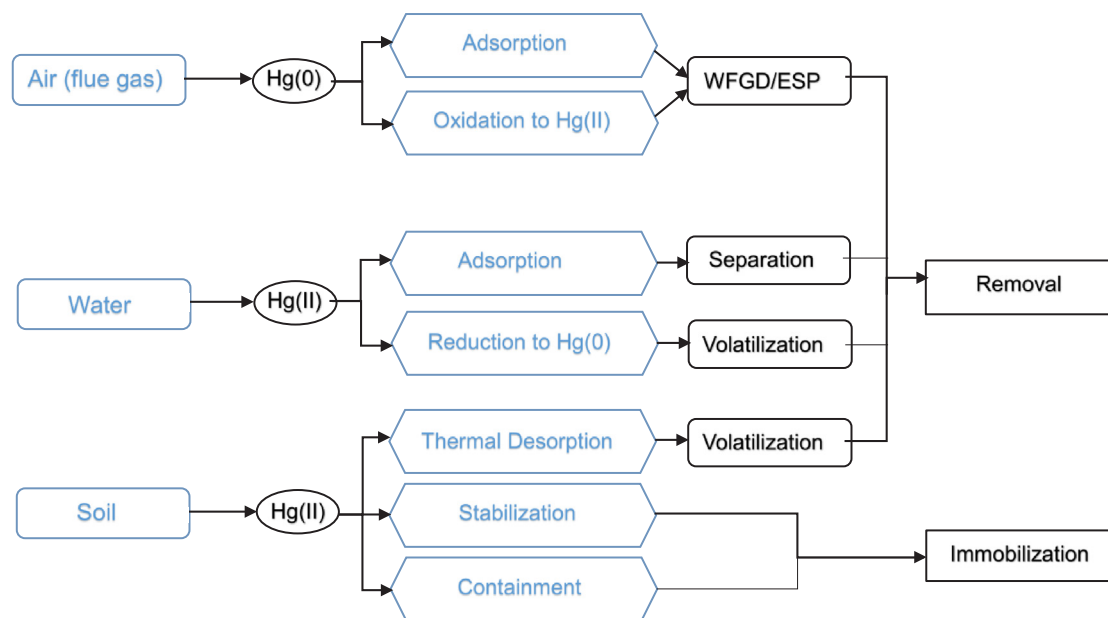

Fig. 2. Major mechanisms involved in Hg remediation. Acronyms: WFGD, wet flue gas desulfurization; ESP, electrostatic precipitation.

(Fig. 2). Removal technologies involve the mechanism of adsorption, desorption, oxidation and reduction. The major aim of these technologies is to separate mercury from the contaminated media or transform toxic mercury species into less toxic ones (Lewis et al., 2016). The most widely adopted immobilization techniques are stabilization and containment, which prevent mercury migration by chemical complexation or physical trapping, respectively (He et al., 2015).

More recent research have been ongoing to develop novel materials and technologies for Hg remediation (Ali et al., 2018; Chen et al., 2018c; Huang et al., 2019b; Moharem et al., 2019; Wang et al., 2019b; Xu et al., 2019). Novel materials, especially materials possessing high surface area, large porosity as well as active sites for adsorption, have been examined extensively in recent studies (Gusain et al., 2019; Kumar et al., 2019). Apart from adsorption capacity which is the key determinant of these materials, other issues such as generation method, stability and reusability should be seriously considered as well (Abraham et al., 2018; Ke et al., 2017; Ram and Chauhan, 2018; Tack et al., 2019). Compared to conventional remediation technologies such as thermal desorption or activated carbon adsorption, innovative

methods have proved to be more cost-efficient and environmentally friendly. Interestingly, most of these technologies treating Hg contaminated soil, water and air can either be based on emerging materials or the metabolism of organisms, namely plants, algae and bacteria.

The aim of this work is to review current knowledge on emerging materials as well as innovative technologies for mercury remediation in soil, water and air. This review discusses the synthesis method, morphology, adsorption behavior, reusability, stability as well as other characteristics of emerging materials. The review also focuses on the remediation mechanisms and remediation efficacy of novel technologies and proposes critical future research directions in this field.

2. Mechanisms involved in mercury remediation

2.1. Adsorption and desorption

Among various methods aiming to remove Hg(II) from water solution, adsorption is the most commonly utilized approach (Fig. 2) (Abbas et al., 2018; Bao et al., 2017; Kyzas and Kostoglou, 2015; Rocha et al.,

2016). The adsorbents usually possess high surface area as well as high porosity and the formation of chelates is the major sorption mechanism (Kyzas and Kostoglou, 2015; Rocha et al., 2016). Mondal et al. (2019b) synthesized thioether-functionalized covalent triazine nanospheres to adsorb Hg^{2+} and $Hg(0)$ from water. Excellent adsorption capability was observed (1253 and 813 mg/g for Hg^{2+} and $Hg(0)$, respectively), and the results of the kinetic study reveal a fast adsorption rate (9 times faster than that of TAPB-BMTTPA-COF and 7 times than PAF-1-SH). Another study by Abbas et al. (2018) synthesized a novel mesoporous conjugate adsorbent based on pentasil zeolite (type ZSM-5) to adsorb Hg(II) in aqueous solution, and the maximum adsorption capacity reached 172.6 mg/g. Bao et al. (2017) utilized silica-coated magnetic nanoparticles to extract Hg(II) from wastewater, and the adsorption of mercury ions onto the imine (C-NH-) groups on the surface of nanoparticles was discovered. Another example used chitosan derivatives as adsorbents. The chelation between Hg(II) and the nitrogen atoms of chitosan is the dominant mechanism of adsorption (Kyzas and Kostoglou, 2015). The mechanism of adsorption is also commonly used for the removal of gas-phase elemental mercury [Hg(0)] (Abraham et al., 2018; Reddy et al., 2015). According to the "hard and soft acid-base" (HSAB) theory, Hg preferentially forms complexes with soft ligands such as sulfur to form insoluble and steady compounds (He et al., 2015). A high sulfur content of an adsorbent was found to promote the adsorption capacity for $Hg(0)$ (Abraham et al., 2018). While using adsorbents for Hg removal, it is of note that stability and reusability should be seriously considered, and more detailed discussion on this issue is provided in Section 3.

When it comes to the remediation of Hg contaminated soil, Hg-containing waste or sludge, thermal desorption has been established as an effective approach (Busto et al., 2011; He et al., 2015; Hung et al., 2016; Lee et al., 2017; Sierra et al., 2016; Wang et al., 2016c; Zhao et al., 2018b). In situ thermal desorption is encouraged, as there is no need to dig up the contaminated environmental media, especially the soil. In this process thermal conductive heating (TCH) elements are inserted into the soil in order to directly transfer heat. (He et al., 2015). During the heating process, the increase of the volatility of mercury results in the separation of mercury from the soil. Various species of mercury exist in soils, such as HgO, HgS, $HgCl_2$, and mercury associated with organic matter (Selin, 2009; Wang et al., 2012). These mercury species are volatilized when the heating temperature is above 600 °C, and the treatment can achieve an acceptable decontamination level (Ma et al., 2015; Wang et al., 2012; Zhao et al., 2018b). The major disadvantage of conventional thermal desorption is the high energy cost, warranting the need for further studies to find low-temperature desorption methods. Many full-scale and pilot-scale applications of thermal desorption have been summarized in other literature (Dermont et al., 2008; He et al., 2015; USEPA, 2007; Wang et al., 2012), and the cost of this technology is estimated to be 480 USD/t soil (He et al., 2015; USEPA, 2007).

2.2. Oxidation and reduction

Coal-fired power plants continued to be the predominant sources of anthropogenic mercury emission to the atmosphere (Bourtsalas and Themelis, 2019; Pirrone et al., 2010). In typical coal combustion flue gas, mercury exist in three forms: elemental mercury [Hg(0)], divalent mercury [Hg(II)] and particulate bounded mercury [Hg(P)]. Among these forms, elemental mercury was recognized to be the hardest to be removed by conventional air pollution control devices owing to its volatility and low water solubility. The oxidation of Hg(0) has proven to be an effective way to decrease mercury emission (Chen et al., 2016; He et al., 2016; Krzyzynska et al., 2018; Liu and Wang, 2018). In most cases, Hg(0) was oxidized to Hg^{2+}, which can be easily captured by an electrostatic precipitator (ESP) or wet flue gas desulfurization scrubbers (WFGD) due to its high solubility and sorption on particulate matter (Li et al., 2012; Liu et al., 2011; Qi et al., 2016; Wang et al., 2010a).

Compared to the adsorption method (i.e. activated carbon injection, around 3–4 USD/kW)(Marczak et al., 2019), oxidation is more cost-effective. A number of studies have focused on a novel oxidation method, i.e., catalytic oxidation of elemental mercury from the flue gas, which will be elaborated in Section 4.3.1. Apart from the catalytic oxidation method, free radical advanced oxidation of Hg(0) is also utilized sometimes (Liu and Wang, 2018; Wang et al., 2010b; Wu et al., 2017a), but Hg(0) removal capacity using this technology remains limited thus far.

Reduction is often applied in order to prevent the formation of methylmercury (MeHg). Methylmercury is the most bioavailable form of mercury. Redox conditions in wetland sediments promote the formation of MeHg (Devai et al., 2005; Frohne et al., 2012; Lewis et al., 2016). A high concentration of Hg(II) species results in the production of MeHg. Therefore, an effective way to control methylmercury production is to decrease the concentration of Hg(II) (Benoit et al., 2001; Hsu-Kim et al., 2013). Zero-valent iron (ZVI) or Fe(II) are often employed to reduce Hg(II) to Hg(0), thus inhibiting MeHg production (Amirbahman et al., 2013; Lewis et al., 2016). Several studies also examined whether adsorbents could provide inhibition of MeHg production. A study by Muller and Brooks (2019) observed that biochar was ineffective at decreasing the total MeHg production in the aqueous phase. Another study by Zhang et al. (2019a) found that particulate-bound Hg(II) is crucial to methylation. In aquatic environments, microbial methylation of particulate-bound Hg(II) should be considered.

2.3. Stabilization and containment

Stabilization approaches immobilize mercury in contaminated sites through chemical complexation to decrease solubility in order to minimize exposure of mercury to the environment (He et al., 2015; Wang et al., 2019a; Wang et al., 2012). During the chemical stabilization process, sulfur-containing reagents such as elemental sulfur, pyrite (FeS_2) or thiosulfate are commonly used to react with Hg(0) in contaminated soil to form HgS, which is very insoluble (solubility product 2.0×10^{-49}) (He et al., 2015; Piao and Bishop, 2006). Soil can be treated either in situ or *ex situ*, the former requiring less energy and labor cost. However, thorough mixing remains very difficult in *in situ* stabilization (Mulligan et al., 2001). A fundamental drawback of stabilization is that mercury is not removed from the contaminated media, thus requiring perpetual future monitoring of the contaminant on site.

Similar to stabilization, contamination is left on site during the containment treatment. Low-permeability physical barriers (e.g. slurry walls, caps or grout curtains) are installed around the contaminated soil to isolate and contain the soil, and thus prevent the migration of mercury to the surrounding environment (Khan et al., 2004). These physical barriers can be divided into three types: capping, vertical barriers and horizontal barriers (Mulligan et al., 2001). The advantages of containment treatment are its relatively low cost (5–15 USD per square foot as vertical barriers)(He et al., 2015) as well as its simplicity, as no excavation and treatment of hazardous waste are involved. The disadvantages of containment are similar to stabilization, and monitoring is also required.

3. Emerging remediation materials

3.1. Nanomaterials

Nanomaterials are gaining more and more attention in mercury remediation of soil, water and flue gas, owing to their high adsorption capacity, small dimension and other unique electrical, mechanical and chemical properties (Alijani and Shariatinia, 2018; Moghaddam and Pakizeh, 2015; Wang et al., 2019d). A range of nanomaterials have been tested for Hg remediation. They can be divided into three types: nanoparticles, nanosheets and nanocomposites (Table 1). The morphology of these materials can vary greatly, as illustrated in Table 2.

Table 1
Characteristics of nanomaterials used in remediation of mercury.

Type	Active constituents	Support material	Size (nm)	Target media	Treated mercury species	Surface area (m²/g)	Adsorption capacity (mg/g)	Reference
C	ZrP	Fe_3O_4	6–10	W	Hg^{2+}	236.62	181.8	(Ahamad et al., 2017)
S	Sulfur atoms	MoS_2	0.94	W	Hg^{2+}	n.a.	2563	(Ai et al., 2016)
C	CoS	SWCNT	70	W	Hg^{2+}	n.a.	1666	(Alijani and Shariatinia, 2018)
C	3-aminopyrazole	MWCNT	24.78	W	Hg^{2+}	166.2	112	(Alimohammady et al., 2018)
C	Oxygen containing groups	MWCNT	12.734	W	Hg^{2+}	199.37	186.97	(AlOmar et al., 2017)
C	Ionized carboxyl and sulfhydryl groups	NC	n.a.	W	Hg^{2+}	116.32	240.0	(Anirudhan and Shainy, 2015)
P	Organic ligand of ammonium	MS	7.2	W	Hg^{2+}	514	164.22	(Awual et al., 2016)
C	Amine and thiol groups	Si-Fe	13.6	W	Hg^{2+}	71.9	355	(Bao et al., 2017)
C	Dithiocarbamate functional group	Si-Fe	93	W	Hg^{2+}	n.a.	82	(Behjati et al., 2018)
C	Nitrogen and amide	Fe_3O_4	17	W	Hg^{2+}	n.a.	86.8	(Bhatti et al., 2018)
P	Gold	FP	13	W	Hg^{2+}	n.a.	99%*	(Chen et al., 2017)
P	Thiol functional group	NC	9.4	W	Hg^{2+}	43.51	718.5	(Geng et al., 2017)
P	EDTA	Fe_3O_4	35	S	Hg^{2+}	n.a.	112	(Ghasemi et al., 2017)
C	Amino and functional groups	MWCNT	9.84	W	Hg^{2+}	234.89	204.64	(Hadavifar et al., 2016)
P	Mn and Fe	CeO_2	7.02	G	$Hg(0)$	108.5	86.5%*	(Jampaiah et al., 2015)
P	Thioglycolic acid	MS	2.35	W	Hg^{2+}	980	42.8	(Kenawy et al., 2018)
P	ZnS	ZnS	6	G	$Hg(0)$	196.1	0.50	(Li et al., 2016)
C	UiO-66-NH_2	Pt	2.48	W	Hg^{2+}	1111.2	206.25	(Li et al., 2017)
C	Fe-Ce mixed oxides	MWCNT	3–5	G	$Hg(0)$	n.a.	69.4%*	(Ma et al., 2018)
P	L-cysteine	FeOOH	14	W	Hg^{2+}	34	217	(Maia et al., 2019)
P	Sulfur atoms	GO	40–80	W	Hg^{2+}	449.43	829.27	(Manna and Raj, 2018)
C	MnO_2	MWCNT	2.7	W	Hg^{2+}	110.38	58.8	(Moghaddam and Pakizeh, 2015)
P	OH and Al-O-Si group	WTR	45–96	S	$Hg_2(OH)_2$, Hg_2CO_3	129.0	93.89%**	(Moharem et al., 2019)
P	Chitosan	Fe_3O_4	10	W	Hg^{2+}	n.a.	10	(Nasirimoghaddam et al., 2015)
P	3-mercaptopropionic acid	NC	45–75	W	Hg^{2+}	404.95	98.6	(Ram and Chauhan, 2018)
C	Polypyrrole	MS	3.1	W	Hg^{2+}	97.6	200	(Shafiabadi et al., 2016)
C	Poly(1-vinylimidazole) oligomer	Si-Fe	10–20	W	Hg^{2+}	n.a.	346	(Shan et al., 2015)
C	Amidoamine	MWCNT	33–42	W	Hg^{2+}	n.a.	101.35	(Singha Deb et al., 2017)
S	Sulfur atoms	MoS_2	0.7–2.4	W	Hg^{2+}	n.a.	425.5	(Song et al., 2018)
P	FeS	NC	n.a.	W	Hg^{2+}	n.a.	1989	(Sun et al., 2018)
P	3,4-dihydroxyphenethylcarbamodithioate	Fe_3O_4	5–20	W	Hg^{2+}	n.a.	52.1	(Venkateswarlu and Yoon, 2015)
P	Magnetic iron-manganese binary oxide	CNF	0.84	G	$Hg(0)$	n.a.	90%*	(Yang et al., 2018a)
P	CuS	CuS	n.a.	G	$Hg(0)$	33.06	122.4	(Yang et al., 2018d)
C	Nanocellulose	Fe_3O_4	21	W	Hg^{2+}	n.a.	926.3	(Zarei et al., 2018)
P	Ce^{4+}/Ce^{3+}	T-A-C	5	G	$Hg(0)$	238.49	80.54%*	(Zhang et al., 2017b)
S	MoS_2	γ-Al_2O_3	10.3	G	$Hg(0)$	177	18.95	(Zhao et al., 2016a)
S	MoS_2	γ-Al_2O_3	0.27	G	$Hg(0)$	n.a.	98%*	(Zhao et al., 2018a)

Acronyms: (1) Type: S = nanosheet; P = nanoparticle; C = nanocomposite; (2) Support material: SWCNT = single-walled carbon nanotubes; MWCNT = multi-walled carbon nanotubes; NC = nanocellulose; MS = mesoporous silica; FP = filter paper; GO = graphene oxide; T-A-C = TiO_2-Al_2O_3-CeO_2; Si-Fe = silica-coated Fe_3O_4 nanoparticles; WTR = water treatment residual nanoparticles; CNF = carbon nanofiber; (3) Target media: S = soil; W = water; G = flue gas.
*Removal efficiency.
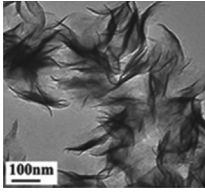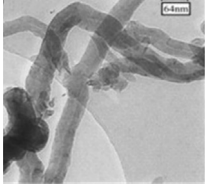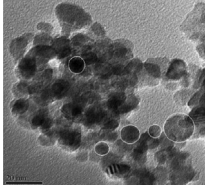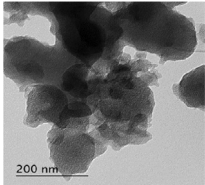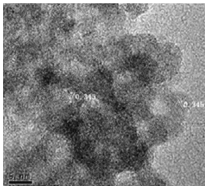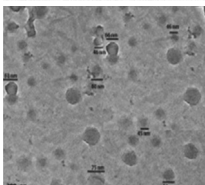**Residual fraction of mercury increased from 69.27% to 93.89%.

Among these types, nanosheets are less frequently used than nanoparticles and nanocomposites, while MoS_2 nanosheets can achieve a high adsorption capacity of both $Hg(0)$ (Zhao et al., 2018a; Zhao et al., 2016a) and Hg^{2+} (Ai et al., 2016; Song et al., 2018).

There are several major types of nanoparticles and nanocomposites. Carbon-based nanomaterials such as carbon nanotubes (CNT) are gaining much interest, and in order to improve their interactivity, amine or thiol groups are introduced through chemical functionalization (Alimohammady et al., 2018; Hadavifar et al., 2016; Singha Deb et al., 2017). Ferroferric oxide (Fe_3O_4) nanoparticles are another emerging material for Hg remediation. They possess some outstanding properties, such as ease of recovery, superparamagnetism and large surface area (Bao et al., 2017; Ghasemi et al., 2017; Zarei et al., 2018). Without further isolation procedures such as centrifugation or filtration, the magnetic nanomaterials can be easily isolated from solutions by an external magnet. Mesoporous silica is also frequently applied owing to a significantly higher surface area-to-volume ratio, but it is rarely used alone without modification (Awual et al., 2016; Kenawy et al., 2018; Shafiabadi et al., 2016). After functionalization of different kinds of nanomaterials, the Hg adsorption ability increases significantly.

The most widely used functional groups to modify the nanomaterials are sulfur, oxygen and nitrogen-containing functional groups such as thiol (−SH), carbonyl (C=O), amino (−NH_2) and cyan (−CN). This is because mercury is a soft acid according to the "hard and soft acid-base" (HSAB) theory, with a high tendency to form strong bonds with these groups (Hadavifar et al., 2016; Li et al., 2017; Maia et al., 2019; Moharem et al., 2019; Singha Deb et al., 2017; Song et al., 2018). The interactions between mercury and these functional groups include electrostatic attraction (Anirudhan and Shainy, 2015), chelation (Bao et al., 2017), ion exchange (Shafiabadi et al., 2016) and chemisorption (Moharem et al., 2019; Singha Deb et al., 2017). Apart from adsorption, oxidation also is an effective approach to treat elemental mercury-containing flue gas. Cerium (Ce) containing nanomaterials are an emerging catalyst for $Hg(0)$ oxidation because of the high standard reduction potential of Ce^{4+}/Ce^{3+} (1.61 V) as well as large oxygen

Table 2
Morphology of the major types of nanomaterials utilized for mercury remediation.

Type	Image	Synthesis process	Surface area (m^2/g)	Pore size (nm)	Adsorption capacity (mg/g)	Hg removal capacity	Reference
MoS$_2$ nanosheet		One-step hydrothermal method	n.a.	0.94	2563	99.8% (initial 10 mg/L Hg^{2+})	(Ai et al., 2016)
Carbon nanotubes (CNT)		Simple hydrothermal synthesis	110.38	2.70	58.8	91.7% (initial 10 mg/L Hg^{2+})	(Moghaddam and Pakizeh, 2015)
Fe$_3$O$_4$ nanoparticle		Simple hydrothermalsynthesis	n.a.	5–20	52.1	97.8% (initial 60 mg/L Hg^{2+})	(Venkateswarlu and Yoon, 2015)
Mesoporous silica		Sol-gel method	980	2.35	42.8	95% (initial 10 mg/L Hg^{2+})	(Kenawy et al., 2018)
Ti-Al-Ce nanoparticle		Sol-gel method	238.49	5	n.a.	80.5% (initial 80 μg/m^3 Hg(0))	(Zhang et al., 2017b)
Nanocellulose		Acid hydrolysis	404.95	45–75	98.6	98.6% (initial 100 mg/L Hg^{2+})	(Ram and Chauhan, 2018)

storage capacity (Ma et al., 2018; Zhang et al., 2017b).

To assure the cost-efficiency, the potential for regeneration of the nanomaterials is a factor of major importance. In most studies reviewed, the adsorbent was regenerated using hydrochloric acid (HCl) (Anirudhan and Shainy, 2015; Behjati et al., 2018; Ghasemi et al., 2017), while other reagents such as EDTA (Singha Deb et al., 2017), thiourea (Kenawy et al., 2018) and H$_2$SO$_4$ (Nasirimoghaddam et al., 2015) can be utilized as well. After Hg desorption by these eluents, nanomaterials can be regenerated by successive washing with deionized water. The adsorbents were dried and reused, but in most cases, the adsorption ability decreased with the increased number of adsorption-desorption cycles (Nasirimoghaddam et al., 2015; Singha Deb et al., 2017).

3.2. Polymers

Polymers have been studied as promising adsorbents for Hg(0) and

Hg^{2+} with high surface area, chemical stability, tunable pore size as well as chemical stability (Aguila et al., 2017). Most of the polymers used certain organic molecules which are easy to functionalize (Table 3). Among these support materials, pillar[5]arene is gaining much attention, for its rich host-guest chemistry with different guests (Cheng et al., 2017; Lin et al., 2017). There are several major generation methods for polymers. Inverse vulcanization is specially employed to make sulfur polymers (Abraham et al., 2018; Parker et al., 2017). Pillar[5]arene based polymers can be formed by self-assembly processes (Cheng et al., 2017; Lin et al., 2017). Free radical polymerization is a more commonly used mechanism and can be applied to form different kinds of polymers, including hydrogel (Karmakar et al., 2019) and porous organic polymers (Aguila et al., 2017). Hydrogel is a kind of 3-D polymeric network which demonstrates kaleidoscopic swelling owing to inherent cross-links (Mondal et al., 2019a). After grafting certain functional groups, hydrogel can adsorb Hg effectively. For instance, a study by Saraydin et al. (2018) used radiation-synthesized

Table 3
Characteristics of polymers used in remediation of mercury.

Active constituents	Support material	Generation method	Treated mercury species (target media)	Geometric size	Adsorption capacity (mg/g)	Reference
Sulfur	–	Porogen and inverse-vulcanisation	Hg(0)(G)	0.17–0.2 mm[a]	0.151	(Abraham et al., 2018)
Thiol group	Porous organic polymer	Free radical polymerization	Hg(0)(G), Hg²⁺(W)	1–10 nm[a]	630 [Hg(0)], 1216 (Hg²⁺),	(Aguila et al., 2017)
L-cysteine	Polypyrrole	Free radical polymerization	Hg²⁺(W)	23.04–29.4 nm[a], 250–400 nm[b]	2042.7	(Ballav et al., 2018)
Polyaniline	Zr(IV) phosphoborate	Sol-gel method	Hg²⁺(W)	n.a.	153.85	(Bushra et al., 2017)
thymine	pillar[5]arene	self-assembly	Hg²⁺(W)	200–300 nm[b]	96%[c]	(Cheng et al., 2017)
Sulfur	1,3-diisopropenyl benzene	Supercritical carbon dioxide	Hg²⁺(W)	10–20 μm[a]	41%[c]	(Hasell et al., 2016)
Terpolymer network hydrogel	–	Free radical polymerization	Hg²⁺(W)	n.a.	1172.97	(Karmakar et al., 2019)
Naphthalimide	Pillar[5]arene	Self-assembly	Hg²⁺(W)	2 μm[b]	98%[c]	(Lin et al., 2017)
Sulfur	–	Inverse-vulcanisation	Hg²⁺(W)	10 μm[b]	84%[c]	(Parker et al., 2017)
Polyethylenimine	Chitosan	One-step crosslinking	Hg²⁺(W)	11.9 nm[a]	1594	(Zeng et al., 2019)

Acronyms: G = flue gas; W = water.
[a] Pore size.
[b] Particulate size.
[c] Removal efficiency.

acrylamide/crotonic acid hydrogel to remove Hg(II) from water. The adsorption isotherm was found to fit the Langmuir model best, indicating the binding sites were homogeneous. Another study by Karmakar et al. (2019) adopted pectin-grafted terpolymer superadsorbent via N-H activated strategic protrusion of monomer, and the adsorption was also found to be monolayer adsorption on homogeneous sites. Porous organic polymers are a burgeoning class of porous material with structural diversity, tunable pore size, high specific surface area and chemical stability (Cheng et al., 2019). However, traditional synthesis of polymers, especially porous organic polymers are environmentally unfriendly, as it involves toxic organic solvents, harsh synthetic conditions and noble metal catalysts. In order to diminish the environmental impact, catalyst-free synthesis is recommended. A study by Peng et al. (2019) synthesized triazine-based porous organic polymers by one-pot amidation polycondensation reaction under mild conditions (atmospheric pressure, 180 °C, catalyst-free). The adsorption capacity of Hg^{2+} reached 229.9 mg/g.

On most occasions, sulfur-containing groups such as thiol and sulfur atoms largely contribute to the adsorption efficiency of mercury. Abraham et al. (2018) prepared a porous sulfur polymer with an adsorption capacity of Hg(0) of approximately 151 μg/g at 60 °C. Aguila et al. (2017) utilized a thiol functionalized porous organic polymer (POP-SH) for the removal of Hg^{2+}, and found that in spite of the high sulfur content of POP-SH, cation-π interactions between Hg^{2+} and the benzene rings of POP-SH also enhanced the adsorption. Apart from increasing the adsorption capability, cation-π interactions can also be employed for the fluorescence detection of Hg^{2+} in water. Lin et al. (2017) generated a supramolecular polymer gel based on naphthalimide functionalized-pillar[5]arene, and found that after adding Hg^{2+}, the polymer gel emitted bright blue fluorescence emission. Other cations cannot induce such fluorescence changes, indicating the ability of this gel to detect Hg^{2+} in water, and the detection limit is 1.65×10^{-9} mol L^{-1} (Lin et al., 2017).

3.3. Biomass and industrial waste-derived materials

In recent years, waste-derived materials have received much attention for their cost-efficiency. Applying these materials to the remediation process is considered a more attractive and environmentally friendly method compared to landfill or incineration (Li et al., 2015c). In general, these materials can be divided into two categories according to the feedstock: industrial waste-derived materials and biomass-derived materials.

Biomass-derived materials include biochar and activated carbon derived from biomass (Table 4). Biochar is a black carbon derived from the pyrolysis of biomass. It is a novel porous material with high surface area, which is beneficial to mercury adsorption and immobilization (Beckers et al., 2019; O'Connor et al., 2018; Tang et al., 2015). The role of biochar in Hg remediation technologies will be discussed in Sections 4.1.2, 4.2.2 and 4.3.4. Activated carbon (AC) is an effective adsorbent removing various inorganic and organic contaminants from different media (e.g. wastewater or flue gas), but its high cost restricts large-scale use (approximately 135,000 USD/t) (Sajjadi et al., 2018). For instance, in flue gas treatment, the annual costs of activated carbon for a 250 MW boiler range from 796,000 to 2,562,000 USD/year, depending on the ESP type, and the annual costs of AC injection were estimated to be in the range of 420,674–20,225,000 USD/kgHg (EPPSA, 2015; Marczak et al., 2019). Generation of AC using waste feedstock therefore is promising. Kazemi et al. (2016) produced activated carbon through chemical activation of wood sawdust, and the surface area of AC reached 1789 m²/g. Another study by Sajjadi et al. (2018) used pistachio wood waste to synthesize AC, with surface area and pore volume 1448 m²/g and 0.901 cm³/g, respectively.

Industrial waste is gaining much concern owing to the large amount of annual production. For example, coal fly ash (CFA) is a by-product of coal combustion of power plants, and the amount of its production is

Table 4

A summary of feedstock and generation methods of various waste-derived materials utilized for mercury remediation.

Material	Feedstock	Generation method	Treated mercury species (target media)	Reference
Zeolite Linde Type A	Coal fly ash	Microwave irradiation	Hg^{2+} (W)	(Attari et al., 2017)
Bioelastomeric foam	Coffee waste	Sugar leaching	Hg^{2+} (W)	(Chavan et al., 2016)
Drinking water treatment residuals	–	–	$HgCl_2$ (S)	(Deliz Quiñones et al., 2016)
Drinking water treatment residuals	–	–	$Hg(OH)_2$ (S)	(Elkhatib et al., 2017)
Biochar	Pine sawdust	Pyrolysis	Hg^{2+}, CH_3Hg^+ (W)	(Huang et al., 2019b)
Activated carbon	Fir wood sawdust	Chemical activation	Hg^{2+} (W)	(Kazemi et al., 2016)
Biochar	Medicine residue	Pyrolysis	$Hg(0)$ (G)	(Li et al., 2015b)
Char	Waste tire	Pyrolysis	$Hg(0)$ (G)	(Li et al., 2015c)
Activated carbon	Wood waste	Chemical activation	Hg^{2+} (W)	(Sajjadi et al., 2018)
Coal fly ash	–	–	$Hg(0)$ (G)	(Yang et al., 2017a)
Halides modified red mud	Red mud	Potassium halides impregnation	$Hg(0)$ (G)	(Yang et al., 2018b)

Acronyms: S = soil; W = water; G = flue gas.

estimated to be 750 million tons worldwide (Attari et al., 2017; Yang et al., 2017a). Attari et al. (2017) synthesized zeolite from CFA, and the average efficiency of Hg^{2+} removal reached 94% with 10 mg/L initial concentration. Apart from CFA, red mud is a by-product of the Bayer Process for alumina production, and the global annual amount of production has reached 160 million tons (Yang et al., 2018b). After impregnation with potassium halides, modified red mud can be used for elemental mercury removal from flue gas. The halides (i.e. KI, KBr) promote the oxidation of captured $Hg(0)$. Waste derived materials have significant potential for use in Hg remediation, but they may contain toxic metals and other contaminants (Bhattacharyya and Reddy, 2012; Hua et al., 2017), and further research should examine the potential risks associated with their application.

3.4. Metal organic frameworks (MOFs)

Made up of metal centers and organic ligands, metal organic frameworks (MOFs) are considered as novel porous crystalline materials possessing high surface areas, tunable porosity as well as availability of in-pore functionality and outer-space modification (Chen et al., 2018a; Huang et al., 2016; Huang et al., 2015b). A variety of generation methods can be utilized for the synthesis of MOFs including hydrothermal synthesis (Chen et al., 2018a; Luo et al., 2015), self-template method (Huang et al., 2015b), one-step carbonization strategy (Huang et al., 2017a) and solvent-assisted linker exchange (Huang et al., 2016), whose basic rule is to simplify the generation procedure to render the use of MOFs more cost-efficient. In order to improve the mercury adsorption capability of MOFs, chemical modification and functionalization in a postsynthetic modification (PSM) strategy is widely operated according to the literature reviewed (Huang et al., 2016; Ke et al., 2017). Sulfur-containing groups are the most frequently used functional groups added to MOFs (Ke et al., 2017; Liang et al., 2018), whose adsorption mechanism is the HSAB rule (see Sections 2.1 and 3.1). Besides adsorption of Hg^{2+} in water bodies, MOFs can also remove $Hg(0)$ in the gas phase by catalytic reactions. Chen et al. (2018a) synthesized a copper based MOF (Cu-BTC) and employed it for the removal of $Hg(0)$ from the sintering gas. It was found that Cu acted as a catalyst for oxidation of elemental mercury: with the existence of HCl, intermediate of CuCl or $CuCl_2$ was formed. After the oxidation of $Hg(0)$ with the aid of chemisorbed O_2, Hg^{2+} reacts with CuCl or $CuCl_2$ and $HgCl_2$ is formed (Chen et al., 2018a). Additionally, the ability of MOFs to remove Hg^{2+} from ultra-low concentration solution (Hg^{2+} concentrations in the ppb magnitude) has gained much interest (Luo et al., 2015; Mon et al., 2016; Xiong et al., 2017). However, recovery of MOFs from water remains a tough challenge (Huang et al., 2015b; Ke et al., 2017; Liang et al., 2016). Besides, stability of MOFs may also be affected by pH and exposure time. A study by Huang et al. (2015a) employed PXRD to examine the stability of a novel MOF, Bi-I-functionalized $Fe_3O_4@SiO_2@$ HKUST-1 under different pH. With the exposure time increasing, some unknown phases were observed with the intensity of PXRD patterns

decreasing, indicating that this MOF material transformed into other phases. In addition, if the solution pH was < 2, this phenomenon was also observed. Owing to the poor stability with time increasing, the large scale use of MOFs is restricted.

3.5. Covalent organic frameworks (COFs)

Covalent organic frameworks (COFs) are novel crystalline porous materials in which building blocks are linked by strong covalent bonds (Ding and Wang, 2013; Song et al., 2019). This type of material is purely constructed with organic building blocks solely from light elements (H, B, C, N and O) (Cote et al., 2005). The rational design of skeletons and pores makes it possible for COFs to combine large porosity, high stability and various functional sites (Ding and Wang, 2013; Huang et al., 2017b). Due to their stability, COFs can act as ideal host materials for other emerging remediation materials. For example, Leus et al. (2018) encapsulated γ-Fe_2O_3 nanoparticles in covalent triazine frameworks, and the adsorption capacity of Hg^{2+} was 165.8 mg/g; apart from high adsorption capacity, chemical stability under ambient conditions increased compared to pristine iron oxide nanoparticles. Another study by Huang et al. (2017b) found that high crystallinity of COFs was retained under harsh conditions such as boiling water, and acidic (6 M HCl) or alkaline conditions (6 M NaOH). In addition to the chemical stability of COFs, it has been discovered that instead of merely being the scaffold, the COF host is able to interact with Hg^{2+} by Hg^{2+}-π interaction, thus promoting the adsorption effect of functional groups (Merí-Bofí et al., 2017; Sun et al., 2017). COFs can also be reused after desorption of Hg. For instance, Leus et al. (2018) washed the adsorbent γ-Fe_2O_3@CTF-1 with 0.1 M thiouria in 0.001% HCl. The adsorption capability of Hg retained in the second sorption test. Another study by Merí-Bofí et al. (2017) used 6 M HCl to remove Hg from the adsorbent (thiol grafted imine-based COFs). Both BET surface area (265 vs 291 m^2/g) and pore volume (0.34 vs 0.41 cm^3/g) decreased, but the reasons for this phenomenon were unclear. In general, COFs are emerging materials with high chemical stability, and further environmental applications of COFs need to be investigated.

3.6. Graphene

Since the discovery of graphene in 2004, this two-dimensional carbon-based material has received much attention owing to its unique structural, mechanical, electrical and adsorption capabilities (Cui et al., 2015a; Kabiri et al., 2015; Novoselov et al., 2004). This material is oxidized to graphene oxide (GO), which can be employed for the adsorption of Hg^{2+} in water solutions. The most widely used generation approach is the modified Hummers' method, which involves chemical oxidation of graphene in H_2SO_4 and $KMnO_4$ (Fu and Huang, 2018; Hummers and Offeman, 1958; Marcano et al., 2010; Tadjarodi et al., 2016). Graphene oxide can act as a nonporous adsorbent, which means adsorption only occurs on its outside surface, thus diminishing the

Table 5
Characteristics and adsorption behaviors of graphene used for Hg^{2+} removal in water.

Type	Modification chemicals	Surface area (m²/g)	Adsorption capacity (mg/g)	Optimum pH	Adsorption isotherm model	Adsorption kinetic model	Reference
GO	2-imino-4-thiobiuret	n.a.	624	5.0	Langmuir	P-2	(Awad et al., 2017)
MGO	Ternary hydrosulphonyl-based deep eutectic solvent	n.a.	215.1	6.0	Langmuir	n.a.	(Chen et al., 2018c)
MGO	EDTA	49.97	268.4	4.1	Freundlich	P-2	(Cui et al., 2015b)
MGO	Xanthate	30.13	118.55	7.0	Langmuir	P-2	(Cui et al., 2015a)
MGO	–	214	16.6	5.0	n.a.	Elovich	(Diagboya et al., 2015)
GO	–	174.3	68.8	6.6	Langmuir	P-2	(Esfandiyari et al., 2017)
MGO	Dithiocarbamate	194.8	181.82	6.0	Langmuir	P-2	(Fu and Huang, 2018)
MGO	–	1259.9	71.3	9.0	Langmuir	P-2	(Guo et al., 2016)
GO	3-mercaptopropyltrimethoxysilane	n.a.	233.17	5.5	BET	n.a.	(Huang et al., 2019a)
GO	Diatomaceous earth	368	500	6.5	Langmuir	P-2	(Kabiri et al., 2015)
GO	Thymine oligonucleotide	n.a.	180.18	7.4	Langmuir	P-2	(Liu et al., 2017)
GO	Silver	251	280.8	5.0	Freundlich	P-2	(Qu et al., 2017)
GO	2-pyridinecarboxaldehyde thiosemicarbazone	n.a.	309	5.0	Langmuir	P-2	(Tadjarodi et al., 2016)
GO	Fe-Mn binary oxides	153.43	32.9	7.0	Sips	P-2	(Tang et al., 2016)

Acronyms: GO = graphene oxide; MGO = magnetic graphene oxide; P-2 = pseudo-second-order.

control of internal diffusion (Esfandiyari et al., 2017). Apart from its high mechanical strength (> 1060 GPa) and theoretical surface area (2630 m² g⁻¹) (Diagboya et al., 2015), GO has various oxygen-containing functional groups such as hydroxyl, carbonyl and carboxyl on its surface, rendering the possibility of covalent modifications with certain chelating groups which have strong tendency of binding with Hg^{2+} (Awad et al., 2017; Chen et al., 2018c). As is mentioned in Section 3.1, adding Fe_3O_4 nanoparticles to GO will facilitate subsequent separation of adsorbent and target media (water) after adsorption, and the utilization of magnetic graphene oxide (MGO) is based on this idea (see Table 5). The magnetic graphene oxide can be produced through co-precipitation (Chen et al., 2018c; Cui et al., 2015a; Diagboya et al., 2015) and other modification chemicals can be added to GO or MGO by sol-gel methods (Chen et al., 2018c; Esfandiyari et al., 2017).

Due to the special single atomic sheet structure of sp²-hybridized carbon atoms, the mercury adsorption isotherms of GO and MGO are mostly Langmuir-type, which may suggest a monolayer adsorption on homogeneous sites (see Table 5). However, several studies have found that experimental adsorption data fit the Freundlich (Cui et al., 2015b; Qu et al., 2017), BET (Huang et al., 2019a) or Sips (Tang et al., 2016) models best, pointing to a multilayer adsorption on a heterogeneous surface. This is probably because the modification chemicals changed the adsorption behavior of graphene oxides, making the surface more complex and heterogeneous. The adsorption kinetics of those GO or MGO materials follow the pseudo-second-order model, indicating a chemisorption process, rather than physical adsorption (Li et al., 2017; Qu et al., 2017). This finding can be confirmed by changing the pH of the solution. The optimum pH mostly falls between 5.0 and 7.0 (Table 5). At lower pH values, the presence of H^+ will cause competitive adsorption (preferential protonation), reducing the amount of Hg^{2+} adsorbed on the surface of graphene oxide (Cui et al., 2015b; Henriques et al., 2016). Under more alkaline conditions, Hg^{2+} is increasingly converted to $Hg(OH)^+$ or $Hg(OH)_2$, which are less prone to chemisorption (Qu et al., 2017).

Apart from conventional regeneration methods using eluents such as EDTA (Chen et al., 2018c; Liu et al., 2017), thiourea (Huang et al., 2019a) and HCl (Cui et al., 2015b; Fu and Huang, 2018), a study by Qu et al. (2017) adopted a thermal decomposition method under 100 °C for 100 min. The released Hg was detected by CVASS. Six cycles of adsorption/desorption tests were conducted, with the Hg^{2+} removal efficiency remaining higher than 95% (initial Hg^{2+} concentration 100 mg/L).

3.7. Layered double hydroxides (LDHs)

Layered double hydroxides (LDHs), also known as hydrotalcite, are a class of two-dimensional (2D) ionic lamellar compounds (Zubair et al., 2017). These materials consist of positively charged metal hydroxide layers as well as exchangeable anions in the interlayer space for charge neutrality (Ma et al., 2017a; Zubair et al., 2017). By intercalating MoS_4^{2-} into the interlayer of LDH, this novel material can be utilized for Hg^{2+} removal from an aqueous phase (Ali et al., 2018; Ma et al., 2017a; Ma et al., 2016). Ali et al. (2018) discovered that the LDH layers protected the inserted MoS_4^{2-} from oxidation, and after intercalation, the structure of LDH was not distorted. The adsorption isotherm best fitted the Langmuir model. Hg^{2+}-S linkages forming a layer between the metallic layers of LDH correspond to the monolayer adsorption assumption of the Langmuir model. This can be proved by other studies, in which a homogeneous monolayer chemisorption mechanism was also investigated (Ma et al., 2017a; Ma et al., 2016). Another study by Yuan et al. (2019) used elemental sulfur to modify LDH, and the result revealed that the unique structure of LDH made it possible to accommodate more polysulfides, indicating an enhanced resistance to SO_2. Owing to the excellent ion-exchange ability as well as the large surface area, this emerging material has received much focus in recent years.

3.8. Minerals

Pyrite (FeS$_2$) has emerged as a cost-effective adsorbent for Hg(0) and Hg^{2+} (Duan et al., 2016; Yang et al., 2018c). Duan et al. (2016) synthesized nano-scale pyrite particles for the removal of Hg^{2+} in water, and found surface precipitation together with adsorption of divalent mercury occurs on the surface of pyrite. Another study by Yang et al. (2018c) used natural pyrite for Hg(0) removal from flue gas. Reactions between adsorbed Hg(0) and S^{2-} monomer on the surface was observed, and the formation as well as the desorption of HgS proved to be the mechanism for Hg(0) removal.

Apart from sulfur-rich minerals, other minerals, especially silicate minerals such as zeolite, vermiculite and clay minerals can also be applied for mercury adsorption. Although raw minerals show poor mercury adsorption capacity, chemically modified minerals have been reported to possess great adsorption abilities (Shao et al., 2016). Compared to other adsorbents such as activated carbon, this kind of material is a low-cost adsorbent, implying possible large-scale applications (Saleh et al., 2018). The major adsorption mechanism of clay minerals (i.e. montmorillonite, vermiculite and palygorskite) is ion exchange (Chen et al., 2015; Tran et al., 2015), while precipitation also plays a vital role in the case of Na-montmorillonite (Chen et al., 2015). Other minerals, such as zeolite and diatomite, possess a highly porous structure, which is beneficial for adsorption after functionalization with certain groups like hexadecyltrimethylammonium bromide (Shirzadi and Nezamzadeh-Ejhieh, 2017), CuBr$_2$ (Liu et al., 2019a) and thiosemicarbazones (Abbas et al., 2018). Removal efficacy of these porous materials depends largely on these groups, and minerals function as the supporting structure of the composite.

3.9. Other materials

Manganese oxides have been reported to possess high Hg(0) removal efficiency from flue gas based on catalytic oxidation of elemental mercury (Scala and Cimino, 2015). The gaseous Hg(0) first is physically sorbed on the surface of Mn-based oxides. After sorption, Hg(0) is oxidized to Hg(II) while Mn is reduced. Finally, the oxidized mercury bind with surface oxygen to form HgO (Ma et al., 2017b). Due to this mechanism, the higher Mn valence species MnO$_2$ has a better oxidation performance than Mn$_2$O$_3$ or Mn$_3$O$_4$ (Ma et al., 2017b). Widely available in the environment, manganese oxides have a low cost, and the environmental friendliness of this material makes it attractive for further applications. Based on the mechanism of oxidation, MnO$_2$ amendments such as birnessite and pyrolusite can be applied in *in situ* remediation of Hg-contaminated sediments (Leven et al., 2018; Vlassopoulos et al., 2018). Microbial sulfate reduction is a fundamental pathway to form MeHg, and manganese oxide amendments can regulate this process through redox manipulation (Vlassopoulos et al., 2018). In heterotrophic microbial metabolism, Mn(IV) reduction was confirmed to be the predominant biogeochemical redox process, and sulfate reduction was suppressed. As a result, MeHg concentrations in pore water decreased by 1–2 orders of magnitude, compared with the control. Apart from Mn oxides, MoS$_x$ chalcogenide aerogels can also be utilized for Hg(0) capture from gaseous phase, where Hg chemically reacted with MoS$_x$ to form HgS. A study by Subrahmanyam et al. (2015) found that Hg atom can be inserted to S−S bonding sites in the aerogel structure to form S−Hg−S units, leading to the high adsorption capacity of chalcogenide aerogels.

Chelating resin can adsorb Hg^{2+} in the aqueous phase through ion exchange, which is the rate-limiting step of adsorption. Xiong et al. (2015) synthesized a novel chelating resin, polyacrylonitrile-2-amino-1,3,4-thiadiazole through a one-step reaction, and the adsorption capacity reached 526.9 mg/g. Additionally, the resin can be regenerated and reused easily by HCl and HNO$_3$. Modified microfiltration membranes can also remove Hg^{2+} from water. A study by Zhang et al. (2018b) fabricated a thiol covered polyamide (nylon 66) microfiltration membrane for the simultaneous removal of oil and Hg^{2+} from wastewater, and discovered that chemisorption between thiol groups and mercury ions according to the HSAB rule was the predominant mechanism for mercury removal. Compared to other thiol-modified materials such as nanomaterials or polymers (Sections 3.1 and 3.2), membranes can be easily separated from water and regenerated using HNO$_3$ solution (Zhang et al., 2018b).

4. Innovative remediation technologies

4.1. Soil and solid waste

4.1.1. Phytoremediation with and without microbial assistance

Compared with other technologies, phytoremediation is a cost-effective and environmentally friendly approach for the remediation of mercury contaminated soil (Lv et al., 2018). Phytoremediation can be conducted at large scale in practical applications, and this technique can also be adopted for hydraulic control (e.g. Superfund Site in Nassau County, New York)(USEPA, 2017). The cost is estimated to be 37–202 USD/m^3 (He et al., 2015; USEPA, 2000b; Wan et al., 2016), which depends greatly on the contaminant removal efficiency, remediation duration and treatment of harvested biomass (Linacre et al., 2005). Phytoremediation involves the use of plants to degrade, extract, volatize or immobilize contaminants from soils, and certain plant species, known as hyperaccumulators, are the essential parts of the remediation process (Chamba et al., 2017; Fernández et al., 2017; Liu et al., 2018a). Hyperaccumulation refers to the ability of a plant to accumulate high concentrations of metals in the above-ground parts (Rascio and Navari-Izzo, 2011). It can either be natural owing to intrinsic features of plants or assisted by microorganisms (Anderson et al., 2005; Franchi et al., 2017).

A number of plant species have been categorized as mercury hyperaccumulators (Chamba et al., 2017). Xun et al. (2017) conducted a pot experiment to examine the capability of the plant species *Cyrtomium macrophyllum* to extract mercury from a mercury contaminated mining area, and found that the mercury concentration reached 36 mg kg^{-1} with the translocation factor of 2.62, and the leaf tissue of *Cyrtomium macrophyllum* showed high resistance to mercury stress. Fernández et al. (2017) conducted a field study using native plant species (*Festuca rubra L., Leontodon taraxacoides, Equisetum telmateya*) for the phytoextraction of mercury in a Hg-As mining area, and discovered that mercury mainly accumulated to higher concentrations in the leaves of the plants, the highest concentration of which reached 84, 78 and 77 mg kg^{-1}, respectively. Concentrations of Hg in different tissues may vary greatly. Typically, the plant accumulates the most Hg in the roots, followed by the leaves and stems (Marrugo-Negrete et al., 2015; Marrugo-Negrete et al., 2016; Molina et al., 2006; Wang and Greger, 2004). Marrugo-Negrete et al. (2016) found that the Hg concentrations in leaves were 2-fold higher than that in stems. This is because the transport function of stems cannot accumulate Hg, and the Hg is transported to the leaves for permanent storage (Marrugo-Negrete et al., 2016).

Sometimes microorganisms play an important role in the phytoremediation process, and among the microorganisms involved in phytoremediation, rhizosphere bacteria has received much attention (Gadd, 2000; Liu et al., 2018a). The rhizosphere bacteria can increase the metal bioavailability in various ways, including altering soil pH, releasing chelators and oxidation/reduction reactions (Franchi et al., 2017; Gadd, 2000). According to Franchi et al. (2017), the efficacy of phytoextraction of Hg was increased up to 45% after the supplementation of plant-associated growth-promoting bacteria (PGPB). By altering metal mobility and bioavailability, the use of PGPB greatly facilitates the phytoremediation process (Glick, 2010).

In general, phytoremediation of mercury contaminated sites is a promising approach because of the low environmental impacts as well as the simplicity of operation. However, phytoremediation will take a

Table 6

A list of production parameters and properties of biochar used for Hg removal in different media.

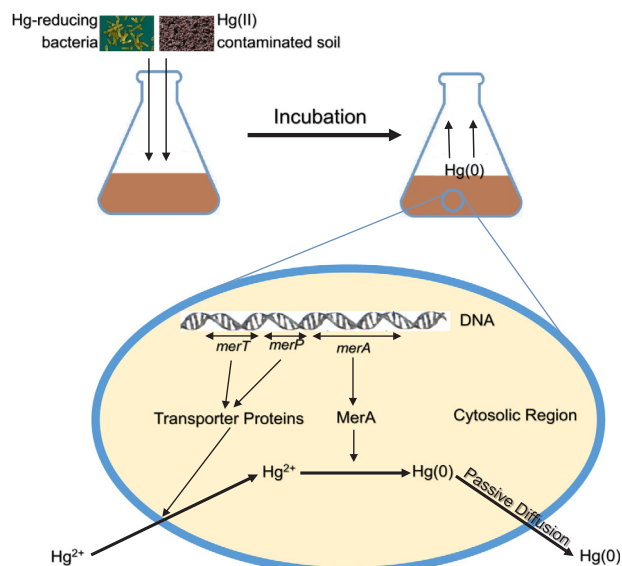| Feedstock	Pyrolysis temperature (°C)	Heating rate (°C/min)	Residence time (min)	Surface area (m²/g)	Pore volume (mL/g)	Treated media	Reference
pine cone	200, 500	7	120	192.97	10.2	soil	(Beckers et al., 2019)
pine sawdust	500	10	120	44	0.051	soil	(Chen et al., 2018b)
rice husk	550	15	120	143	0.042	soil	(O'Connor et al., 2018)
pine sawdust	700	10	180	335.40	0.152	water	(Huang et al., 2019b)
pine sawdust	500	10	180	52.25	0.026	water	(Huang et al., 2019b)
wheat straw	600	n.a.	60	4.5	0.0092	water	(Tang et al., 2015)
pine sawdust	400	5	60	80.35	0.18	water	(Wang et al., 2018a)
cotton straw	600	n.a.	60	203.7	0.162	flue gas	(Li et al., 2015d)
municipal solid waste	600	n.a.	120	12.4	0.040	flue gas	(Li et al., 2015a)
herb medicine residue	600	20	60	24.92	0.0375	flue gas	(Li et al., 2015b)
seaweed	800	20	20	26.20	0.034	flue gas	(Liu et al., 2018b)
herb medicine residue	600	20	60	24.9	0.0375	flue gas	(Shen et al., 2015)
waste tea	500	n.a.	120	142.05	0.086	flue gas	(Shen et al., 2017)
tobacco straw	600	10	60	8.2	n.a.	flue gas	(Wang et al., 2018b)
rice straw	600	n.a.	20	26.66	0.121	flue gas	(Xu et al., 2018)
seaweed	800	n.a.	20	21.15	0.466	flue gas	(Xu et al., 2019)
wheat straw	600	n.a.	20	65.151	0.184	flue gas	(Yang et al., 2017b)

long time in most cases, and the remediation efficiency is limited by the depth of the root as well as the bioavailability of the heavy metal. After harvest, how to deal with the biomass containing mercury is a tough problem and may cause health risks if not properly treated.

4.1.2. Immobilization with biochar and other amendments

A few studies investigated the effect of biochars on immobilizing Hg in soil (Table 6). For instance, a fully-crossed small plot study by Gilmour et al. (2018) applied pine dust biochar in immobilizing MeHg in a salt marsh, and found that the application of biochar did not reduce total Hg, and that the removal efficiency of MeHg was not satisfactory. However, the application of sulfur-modified biochar proved to be an ideal approach to reducing Hg^{2+} in contaminated soil (O'Connor et al., 2018). Rice husk was modified with non-toxic elemental S, which increased the biochar's Hg^{2+} adsorptive capacity by 73%, to 67 mg/g, and the treatment dosage of 5% (dry wt.) reduced 99.3% of freely available mercury in TCLP leachates compared to untreated soil (O'Connor et al., 2018). Apart from biochar, other immobilization amendments were also utilized for the remediation of methylmercury, such as activated carbon (Gilmour et al., 2018) and activated clay (Yin et al., 2016). When it comes to the immobilization of Hg(0), selenium nanoparticles turned out to be effective (Wang et al., 2019c; Wang et al., 2017b). Under aerobic and anaerobic conditions, selenium nanoparticles converted 45.8–57.1% and 39.1–48.6% of the Hg(0) in the soil to the insoluble mercuric selenide (HgSe), respectively (Wang et al., 2017b). The addition of biochar and other immobilization amendments is innovative, and mechanisms of Hg-immobilization are still not fully understood. In addition, we argue that field studies be conducted to examine the feasibility of these immobilization amendments in real occurrences.

4.1.3. Microbial reduction and volatilization

Because Hg^{2+} in soil could be converted to the most toxic form methylmercury, reducing Hg^{2+} to elemental mercury Hg(0) is considered to be detoxification (Wagner-Dobler, 2003). Mercury resistant bacteria are used in this microbial reduction and volatilization process, because they possess the *mer* operon (Nascimento and Chartone-Souza, 2003). The *mer* operon carries a number of genes and gene products closely related to the mercury tolerance and reduction mechanism of these bacteria (Mahbub et al., 2016; Mahbub et al., 2017; Mathema et al., 2011; McCarthy et al., 2017). As is shown in Fig. 3, *merP* and *merT* genes express transporter proteins which enable Hg to enter the cytoplasm. Then the mercuric reductase enzyme encoded by *merA* reduces Hg^{2+} to Hg(0), which diffuses passively out of the cell (Chen

Fig. 3. A conceptual figure for microbial reduction and volatilization of mercury. MerA: the mercuric reductase enzyme encoded by *merA* gene.

et al., 2018d; Quinones et al., 2013). In some bacteria *merB* gene expresses organomercury lyase enzyme, which can break the C—Hg bound in organic compounds, making the mercury ion available for the reduction (Barkay et al., 2003). Mahbub et al. (2016) used a highly Hg resistant strain *Sphingobium* SA2 for reduction and volatilization of mercury, and 79% of mercury was volatilized in 6 h. Another research conducted by Mahbub et al. (2017) found 44% removal rate within 6 h dominated by *Sphingopyxis* sp. SE2. In order to improve the bioavailability of mercury, Chen et al. (2018d) utilized a chemical extraction procedure before bacteria reduction. Ten hours of ammonium thiosulfate (0.5 M) extraction was used to extract mercury from the soil to the water phase. Then reduction of Hg^{2+} was conducted and the removal rate reached 81%. Compared to a one-stage method that only involves bacterial reduction and volatilization, the two-stage approach is not a cost-effective and green method for remediation. How to increase the removal rate of mercury using simpler methods deserves further investigation.

4.1.4. Electrokinetic removal

Electrokinetic remediation is frequently employed to remove

mercury from low permeability clay soils or sediments (Wang et al., 2012). Electrodes are directly inserted into the contaminated soil and low-intensity direct current is applied. Under this electric field (voltage gradient < 100 V/m), cations will migrate towards the cathode, while anions will move to the anode through three mechanisms: electroosmosis, electromigration and electrophoresis (Essa et al., 2015). On most occasions, electrodes are placed in specifically constructed compartments containing an electronic solution, and by ionic migration the dissolved mercury species accumulate in the compartment. The mercury subsequently can be removed by extracting the solution in the compartment or by precipitation (Rosestolato et al., 2015). Electrokinetic removal efficiency is strongly hampered by the low solubility of mercury in soil. Attempts to enhance the removal efficiency have involved adding chemicals that improve the solubility of mercury. Robles et al. (2015) added EDTA as an enhancing solution, and the formation of a strong Hg-EDTA complex ($[Hg–EDTA]^{2-}$) contributed to the migration of mercury to the anode. After entering the anode compartment, a second treatment to remove Hg(II) from the aqueous phase was applied using a permeable reactive barrier (PRB). Sometimes electrokinetic remediation can be combined with adsorption using adsorbents like granular active carbon (GAC) (Essa et al., 2015; Mu'azu et al., 2016). By inserting chambers filled with adsorbents between the two electrodes, mercury can be adsorbed when migrating, thus promoting the removal efficiency (Essa et al., 2015). However, the relatively high energy cost, the acidic conditions required for this technology as well as the interfering effect of other ions during the remediation process has restricted its field-scale application (Wang et al., 2012). The cost of this process is estimated to be 177 USD/m^3 (USEPA, 2007).

4.1.5. Constructed wetlands

Owing to the low cost of maintenance and operation (48–67 USD/m^2) (Gunes et al., 2011; USEPA, 2000a), constructed wetlands are a feasible way for mercury remediation. The mechanisms for mercury removal in constructed wetlands are complex. Major mechanisms include binding to soils and sediments (through coagulation and flocculation, ion exchange, adsorption oxidation and reduction), precipitation, phytoremediation by macrophytes, and microbial metabolism (Bachand et al., 2019; Gomes et al., 2014; Marrugo-Negrete et al., 2017). For example, a study by Bachand et al. (2019) examined the Hg removal efficiency from surface waters using constructed wetlands enhanced by Al and Fe coagulation treatments (i.e. polyaluminum chloride and ferric sulfate), which indicated that floc formation and methylation suppression was responsible for the Al and Fe treatment behavior, respectively. Another study conducted by Gomes et al. (2014) utilized an aquatic macrophyte, *Typha domingensis* for phytoremediation of water contaminated with mercury in a constructed wetland with subsurface flow, whose transfer coefficient reached 7751 L kg^{-1}.

However, it is of note that wetlands are hotspots for Hg methylation, as has been discussed in Section 2.2. For instance, Feng et al. (2014) observed that if the sulfate concentration in inflow water is high (59.9 mg/L), the activity of sulfate-reducing bacteria will be stimulated and subsequently lead to MeHg formation in the wetland ecosystem. Another study by Zheng et al. (2013) found that dryout and rewetting events also promoted Hg methylation and the release of both THg and MeHg from the soil to surface water. Moreover, the uncertainty of this technology cannot be neglected and constructed wetlands are time-consuming compared to other technologies. The plants in the wetland ecosystem constructed by García-Mercadoa et al. (2017) died before the end of the treatment for unknown causes and the removal efficiency of mercury from contaminated soil was not satisfactory (55–71% removed over 36 weeks). Further research may focus on the mercury transformation and fate in the constructed wetland to better understand the remediation mechanism, and the role of microorganisms (as mentioned in Section 4.1.3) in this ecosystem should be examined (especially sulfate-reducing bacteria involved in MeHg processes), instead of merely relying on macrophytes or chemical treatment.

4.1.6. Enhanced thermal desorption and soil washing

As is mentioned in Section 2.1, thermal desorption of mercury can attain an acceptable decontamination level when the heating temperature is above 600 °C. With the aim of reducing the energy cost, thermal desorption can be enhanced by chemicals that can react with hardly volatile mercury species. Citric acid, a natural low-molecular-weight organic acid, was shown to allow reducing the heating temperature to 400 °C (Ma et al., 2015). This is explained by the acidic environment provided by citric acid, which facilitated desorption of mercury cations from the surface of soil particles. Treating contaminated soil (initial concentration 134 mg/kg) for 60 min reduced the mercury concentration to 1.1 mg/kg. Also using FeCl$_3$ the heating temperature can be reduced, which is attributed to the formation of mercury chlorides with low boiling points (Ma et al., 2014). Moreover, both citric acid and FeCl$_3$ treated soils retained most of the physico-chemical properties, indicating the possibility for agricultural reuse (Ma et al., 2015; Ma et al., 2014).

Soil washing can permanently remove contaminants from soil *via* physical separation or chemical leaching (Wang et al., 2012). In situ soil washing can avoid the risks associated with contaminant transport during off-site treatment, but one has to make sure that all leachate is recovered, and not leached out in neighboring soil and groundwater (He et al., 2015). Although water alone can be utilized as the washing solution, chemicals such as HCl, HNO$_3$, EDTA and Na$_2$S$_2$O$_3$ are often added during the washing process in order to improve the Hg removal efficiency (Han et al., 2019; Rodriguez et al., 2012). Han et al. (2019) examined the leaching behavior of sodium thiosulfate treated Hg-contaminated soil, and found that more than 90% of weak acid-soluble and reducible mercury could be extracted based on BCR analysis (initial total mercury content 1100 mg/kg). Generally, soil washing is suitable for soils with high permeability (i.e. sandy or silty soils). However, the disadvantages include: (1) not suitable for low permeability soils (e.g. clay); (2) the high water consumption for the washing process; (3) extracted mercury enters the washing solution, which requires water treatment before discharge.

4.2. Water and wastewater

4.2.1. Algae-based Hg removal

The application of marine macroalgae is a cost-effective technology for mercury removal from saline waters (Henriques et al., 2015). Marine algae can be divided into three categories: brown algae (Phaeophyta), red algae (Rhodophyta) and green algae (Chlorophyta), the differences of which lie in the cell wall, indicating binding preferences for different metals (Romera et al., 2007). A study by Henriques et al. (2015) investigated the Hg^{2+} removal efficiency of three types of algae, and found that *Ulva lactuca*, a green macroalgae which possesses several functional groups such as hydroxyl, amino, sulfate and carbonyl, performed best. Mercury removal is attributed to both bioaccumulation by the living organisms and biosorption on the biomass, either from living or non-living algae. Compared to bioaccumulation, biosorption by dried biomass is a much quicker process, because only physicochemical mechanisms account for the Hg adsorption. However, the utilization of living macroalgae showed better removal efficiency, because the adsorbed mercury was transported into the cells, freeing the binding sites for subsequent adsorption (Henriques et al., 2015). Upon accumulation, Hg will bind strongly in macroalgae tissues without being transferred to more toxic species such as methylmercury, which was also found in another study (Henriques et al., 2017). In both studies, the bioconcentration factor of mercury was as high as 2000 (Henriques et al., 2017; Henriques et al., 2015), indicating great mercury accumulation ability of *Ulva lactuca*. However, discrepancy exists whether Hg will not be transferred into MeHg by algae. Lei et al. (2019) found that algal organic matter enhanced the abundance of microbial methylators, thus raising MeHg concentrations in a eutrophic lake. This discrepancy may be due to the algal species, and deserves further

investigations. Besides, this technique can only be applied when the initial concentration of Hg^{2+} exerts no critical toxic effect to cells (both studies adopted an initial concentration of 100 µg/L), which has limited its application.

4.2.2. Biochar-based Hg removal

Eco-friendly biochars are regarded as promising adsorbents for mercury removal from water, and biochar based Hg removal is an innovative technology due to its excellent removal efficiency as well as cost-efficiency and environmentally friendliness (Boutsika et al., 2014; El Hanandeh et al., 2016; Faheem et al., 2018; Jia et al., 2019). The active sites on the surface of biochar such as −OH, C=O, π bond and C−O make it possible for chemical modification of biochar by adding thiol or amino groups with the aim of enhancing the adsorption capability (Huang et al., 2019b). Chemical binding of Hg^{2+} and surface active sites (e.g. −SH, −NH$_2$, −OH, −COOH) is the major mechanism of adsorption (Huang et al., 2019b; Liu et al., 2016; Tang et al., 2015). It is noteworthy that biochars derived from different feedstocks may greatly influence the adsorption behavior, according to Liu et al. (2016). The results of X-ray absorption indicate that mercury binds to S in sulfur-rich biochars, and to O and Cl in biochars with low sulfur content. Feedstock will not only affect the binding mechanism of biochars, but also sulfate concentrations in the aqueous phase, which may restrict the utilization of certain types of biochars for mercury removal. This is because the raised SO_4^{2-} concentrations released from biochar (up to 1000 mg/L) can be used as electron acceptors, thus enhancing the activity of sulfate reducing bacteria, which are regarded as major Hg methylators (Hsu-Kim et al., 2013). It has been reported that biochar produced from poultry manure or mushroom soil will elevate sulfate concentrations, so special care must be taken when selecting the feedstock of biochars to prevent the release of sulfate when treating mercury contaminated water (Liu et al., 2016). But results of Muller and Brooks (2019) indicate that SO_4^{2-} concentration (1–65 mg/L) did not influence Hg methylation. It is hypothesized that this discrepancy may be due to the variance of released SO_4^{2-} concentrations.

4.2.3. Photocatalytic nano-array

When it comes to Hg^{2+} detection in wastewater, surface enhanced Raman spectroscopy (SERS) is a simple technique (Chen et al., 2012). Based on the interaction of Hg^{2+} ions with SERS active metal nanoparticles, high selectivity towards Hg^{2+} together with high sensitivity (order of µg/L) can be achieved. In the light of this mechanism, Kandjani et al. (2015) synthesized SERS active ZnO/Ag nano-arrays for both Hg^{2+} detection and removal from wastewater (Fig. 4). Initially, the ZnO layer was prepared through sol-gel method, and then ZnO nano-arrays were grown by soft hydrothermal method. Finally silver nanoparticles were merged with the nano-arrays via electroless plating. The intensity variation of the Raman band at 1358 cm^{-1} and the photocatalytic reduction of Hg^{2+} to Hg(0) by ZnO/Ag arrays account for the detection and the removal mechanism, respectively. The regeneration of nano-arrays, by heating at 150 °C for 2 h under vacuum, is rather easy. On the whole, this remediation technology shed light on the simultaneous detection and removal of Hg^{2+}, and the reusability of nano-arrays makes this technology cost-effective.

4.3. Air and gas

4.3.1. Catalytic oxidation and removal

As depicted in Section 2.2, removal of elemental mercury from gaseous phases, especially coal combustion flue gas, can be accomplished by oxidation. Chen et al. (2016) synthesized IrO_2 modified Ce-Zr solid solution catalysts to achieve the effective catalytic oxidation of elemental mercury. It was found that Hg(0) was first oxidized to HgO with the help of surface chemisorbed oxygen species. After this process, HgO could either desorb from the catalysts by itself or react with HCl to be released in the form of gaseous $HgCl_2$ (Chen et al., 2016). Another

study by He et al. (2016) also found that oxidation was enhanced by HCl as a result of the Deacon mechanism. Recently, photocatalytic oxidation has gained much concern. Under ultraviolet or visible light irradiation, a semiconductor is capable of absorbing photons that excite electrons from the valence band to the conduction band (Qi et al., 2016; Wu et al., 2018a). During this process, the induced electrons (e$^-$) and positively charged holes (h$^+$) on the surface of the semiconductor material can induce more reactive constituents, such as the hydroxyl radical (˙OH) (Jiang et al., 2016; Qi et al., 2016) or superoxide radical (˙O$_2^-$) (Zhang et al., 2017a), which effectuate the oxidation of Hg(0) to Hg(II). One typical photocatalyst is TiO_2 (Wu et al., 2018a). However, owing to the wide energy band gap (3.2 eV) of TiO_2, this catalyst can only be aroused by UV irradiation. In order to overcome this drawback, the effect of Bi based photocatalysts which can be activated by visible light irradiation on Hg(0) oxidation have been examined (Jiang et al., 2016; Qi et al., 2016). According to Qi et al. (2016), the photo-generated holes (h$^+$) on the surface of $BiOIO_3$ catalyst were the dominant oxidation species responsible for Hg(0) removal. Another study by Jiang et al. (2016) fabricated a $BiOI/BiOIO_3$ composite as the photocatalyst, and found that the stability of this catalyst is satisfactory, which can be used for at least 5 times without obvious change of removal efficiency. Apart from Bi based photocatalysts, Ag based catalysts such as Ag_2CO_3 (Zhang et al., 2017a), AgCl (Zhang et al., 2018a) can oxidize Hg(0) under visible light. In general, catalytic oxidation, especially photocatalytic oxidation induced by visible light, has a broad application prospect for elemental mercury removal.
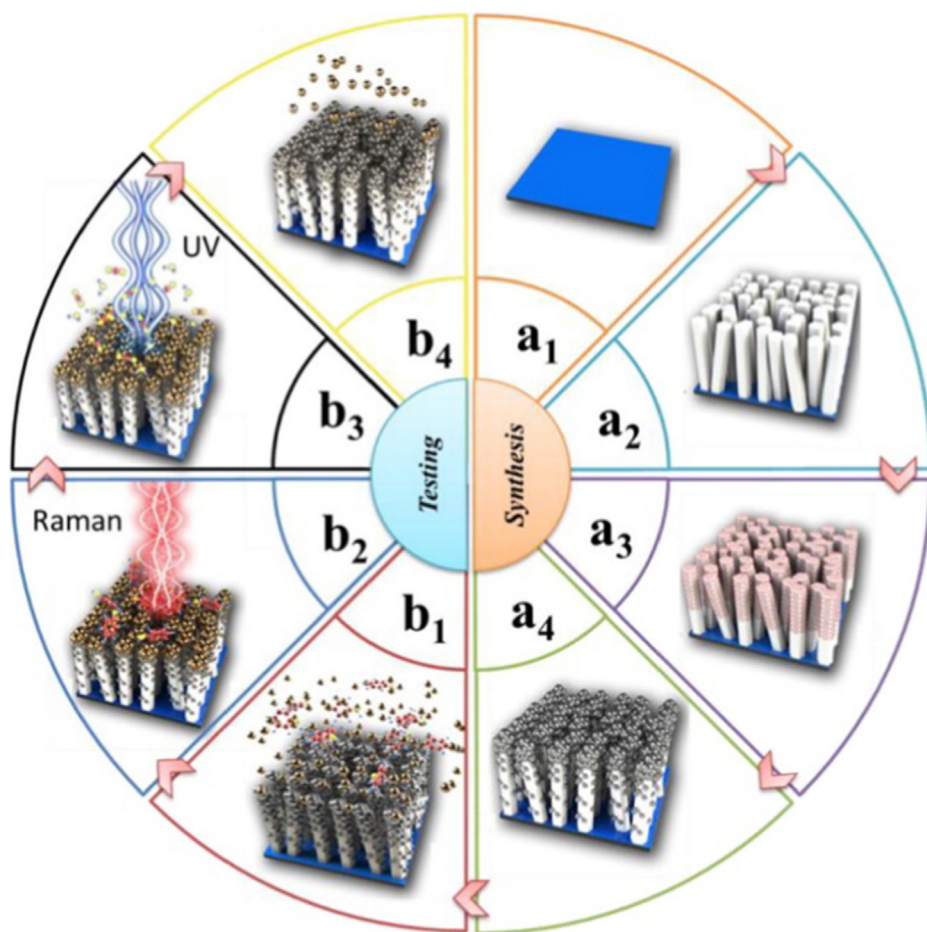
4.3.2. Co-removal of NO and Hg

Selective catalytic reduction (SCR) is widely applied in power plants to remove NO$_x$ from the flue gas (Wang et al., 2017a). In addition to the effective removal of NO, the catalyst used in the SCR process facilitates the oxidation of elemental mercury [Hg(0)] into divalent mercury [Hg(II)], which can be consequently separated from the gaseous phase (Table 7) (Ma et al., 2018). The synergistic conversion process offers a possibility for simultaneous removal of Hg(0) and NO under relatively low temperature within the range of 175 °C and 400 °C, which is determined by the characteristics of the commercial catalysts utilized for the SCR process (Zhang et al., 2015; Zhao et al., 2016b). The traditional SCR catalysts such as V_2O_5 or TiO_2 can be modified by cerium (Ce), which is because of the high redox ability of Ce^{4+}/Ce^{3+} couple (standard electrode potential 1.61 V) (Chi et al., 2017; Gao et al., 2018; Wang et al., 2017a). This modification method can also be utilized to synthesize nanomaterials for mercury removal (see Section 3.1).

According to the literature reviewed, co-existing constituents in the flue gas will impact the co-removal efficiency. For instance, Hg(0) oxidation was inhibited with increasing concentration of NH$_3$ (Chi et al., 2017) or SO$_2$ (Li et al., 2018) but enhanced in the presence of O$_2$ (Liu et al., 2019b; Zhang et al., 2015). This phenomenon can also be found in other types of flue gas mercury removal technologies like biochar-based Hg removal (see Section 4.3.4). Notably, the concentration of NO will also influence the Hg oxidation performance of catalysts, as a high NO concentration will exert toxic effects to the catalysts, thus reducing the removal efficiency of mercury (Zhang et al., 2017c). So care must be taken if SCR is used to remove Hg(0), and an optimum NO concentration as well as temperature will ensure the removal efficiency of elemental mercury.

4.3.3. Advanced oxidation

Advanced oxidation has gained much attention for Hg(0) control and multicomponent flue gas purification. During this process, the hydroxyl radical (˙OH) together with other reactive oxygen species including superoxide (˙O$_2^-$) and hydrogen peroxide (H_2O_2) are generated, all of which possess a high oxidation potential (Liu and Adewuyi, 2016). There are four major types of advanced oxidation technologies (AOTs), namely, plasma AOTs, TiO_2 photocatalytic AOTs, photochemical AOTs and activated oxidant AOTs (Liu and Adewuyi,

Fig. 4. Detailed (a) Synthesis and (b) Sensing, Removal and Regeneration Processes, Starting with (a1) ZnO Seed Layer synthesis through Sol-Gel method, (a2) ZnO Hydrothermal Array Growth, (a3) Decoration of the Nano-Arrays with Palladium Nanoparticles by Charge Exchange Between Sn^{2+} and Pd^{2+} at the Surface of the ZnO Nano-Arrays, (a4) Performing Silver Electroless Plating Decorating the ZnO Arrays; Followed by, (b1) Adsorption of Hg^{2+} Ions on ZnO/Ag Nano-Arrays and Subsequent Adsorption of Raman Marker on the Arrays, (b2) Raman Detection of Marker on Mercury Contaminated ZnO/Ag Nano-Arrays, (b3) Photocatalytic Degradation of Marker Dye and Finally, (b4) Removing Mercury Contamination from the ZnO/Ag Nano-Arrays by Using Heat Treatment under Vacuum As the Regeneration Step. Reprinted with permission from Ref. (Kandjani et al., 2015). Copyright 2015 American Chemical Society.

2016). Of these, activated oxidant AOTs are the most promising owing to the low energy consumption as well as the high oxidation capability. A study by Liu et al. (2015) added Fe^{2+} to H_2O_2 solution so as to form a fenton system, and it was found that Hg(0) was oxidized by $\cdot OH$ and H_2O_2 in fenton solution. Another research by Liu and Wang (2019) used vacuum ultraviolet light (VUV) to activate the $O_3/H_2O/O_2$ system, and the $\cdot OH$ together with $SO_4^{-} \cdot$ was found to be responsible for Hg(0) oxidation. This technology is regarded as an environmentally friendly method for Hg(0) removal. However, there still exist some challenges for industrial applications.

4.3.4. Biochar-based flue gas treatment

A number of studies investigated the effect of Hg(0) removal in flue gas based on modified biochars (Table 6). Certain functional groups (e.g. C—O, C—Cl, C—I, C═O) proved to be the activated sites and improved the Hg(0) removal efficiency (Li et al., 2015a; Li et al., 2015b; Li et al., 2015d; Liu et al., 2018b; Shen et al., 2017; Wang et al., 2018b; Yang et al., 2016). After pyrolysis of biochars, physical activation such as microwave (Shen et al., 2015) or non-thermal plasma (Wang et al., 2018b) can be utilized to increase the number of active sites, improve pore structure and introduce certain functional groups. However, researchers have found that chemical activation and chemisorption are much more important for the removal of Hg(0) (Li et al., 2015d). Modifying the biochar using NH_4Cl was found to be an optimal modification approach because of high efficiency and low price (Li et al., 2015a; Li et al., 2015b; Li et al., 2015d; Shen et al., 2015; Shen et al., 2017; Xu et al., 2019; Zhu et al., 2016). The removal of Hg(0) by NH_4Cl impregnated biochars was due to the C—Cl generation on the surfaces of biochars, which may transform Hg(0) to $HgCl_2$ or other Hg—Cl complexes. XPS analysis proved the theory that most of the combined C—Cl groups on the surface of biochars were changed to ionic Cl during the chemisorption process (Li et al., 2015a; Li et al., 2015d). Apart from NH_4Cl, other chemicals such as NH_4Br, KI, KCl, KBr could also modify biochars to attain a better capability of removing Hg(0) (Liu et al., 2018b), and halogen plays an important role in chemisorption. Several studies also examined the effects of biochars modified by CuO_x and CeO_2 (Xu et al., 2018) and Mn-Ce mixed oxides (Yang et al., 2017b), which are regarded as promising catalysts for the oxidizing of Hg(0). In recent years, magnetic biochars (MBC) have gained much attention in flue gas Hg(0) treatment. Yang et al. (2016) discovered that it is the C═O group that act as electron acceptors, thus promoting the electron transfer for Hg(0) oxidation. In addition, Fe_3O_4 in MBC acts as adsorption/oxidation sites for Hg(0) reaction, resulting in the formation of $Hg–Fe_3O_4$.

Biochar-based flue gas treatment is a promising approach to remove Hg(0), but other constituents in the flue gas will have an effect on the removal efficiency. It is reported that O_2 and NO in the flue gas promoted the Hg(0) removal, while high concentrations of H_2O and SO_2 inhibited this process (Xu et al., 2018; Xu et al., 2019; Yang et al., 2017b). Thus a new modification method which can diminish the influence of other components in the flue gas is needed.

5. Challenges and future research directions

Traditional remediation technologies have been applied widely for mercury removal, despite some significant disadvantages. Firstly, the high cost of some methods such as thermal desorption and adsorption by activated carbon is an obstacle for large-scale applications (Gilmour et al., 2018; Ma et al., 2015). When it comes to mercury stabilization and containment in soil using technologies that are suited for application on large sites, long-term monitoring of the stability of mercury should be conducted (Wang et al., 2012).

Table 7
NO and Hg removal performances under different SCR conditions.

Catalyst	Temperature (°C)	gas hourly space velocity (h^{-1})	Initial flue gas NO concentration	NO removal efficiency (%)	Initial flue gas Hg concentration	Hg removal efficiency (%)	Reference
Ce-Cu modified V_2O_5/TiO_2	200–350	45,000	500 ppmv	97	30 $\mu g/m^3$	75	(Chi et al., 2017)
activated coke granules loaded with La_2O_3-CeO_2	180	5000	800 ppmv	91.3	80 $\mu g/m^3$	94.3	(Gao et al., 2018)
CoO_x modified MnO_x/biomass activated carbons	240	180,000	500 ppmv	86.5	400 $\mu g/m^3$	98.5	(Gao et al., 2019)
MnO_x/CeO_2-TiO_2	175	10,200	400 ppmv	> 99.5	50 ppbv	90	(He et al., 2013)
Nb-modified $MnTiO_x$	200	108,000	500 ppmv	99	75 $\mu g/m^3$	97	(Liu et al., 2019b)
Fe – Ce Mixed Oxides Supported on Carbon Nanotubes	240	30,000	1000 ppmv	99.1	n.a.	88.9	(Ma et al., 2018)
ZrO_2 modified CuO-CeO_2/TiO_2	250	50,000	500 ppmv	83.3	100 $\mu g/m^3$	72.7	(Wang et al., 2017a)
V_2O_5-CeO_2/TiO_2	250	65,000	500 ppmv	91.2	60 $\mu g/m^3$	81.6	(Zhang et al., 2015)
MnO_x/TiO_2	240	50,000	400 ppmv	80	60 $\mu g/m^3$	80	(Zhang et al., 2017c)
Ce-Mo/TiO_2	300	119,000	600 ppmv	99	145 $\mu g/m^3$	94	(Zhang et al., 2019b)
V_2O_5/ZrO_2-CeO_2	250	100,000	700 ppmv	87.3	70 $\mu g/m^3$	77.6	(Zhao et al., 2016b)

The major mechanism for Hg removal by emerging remediation materials is adsorption. Various materials with high specific area, large porosity and active sites for mercury are explored in numerous studies. Although features such as specific area, pore size and adsorption capacity have been thoroughly investigated to reveal the characteristics of sorbents, it is suggested that future research focus on the partition coefficient of Hg species to compare the adsorption efficiency of different materials easily. In addition, more studies should be conducted to examine the adsorption efficacy of these sorbents in environmentally relevant solutions, as solution chemistry affects their adsorption performance greatly. For instance, dissolved organic matter (DOM) strongly affects Hg speciation, transformation and reactivity in natural waters. The complexation of Hg(II)-DOM can make Hg(II) unavailable for adsorption (Johs et al., 2019). Under sulfidic conditions, microbial methylation can be enhanced owing to the increased bioavailability of Hg(II)(Graham et al., 2012). Besides, other co-existing metal ions may cause competitive adsorption, thus affecting the adsorption performance (Leus et al., 2017). In order to reduce the cost, waste-derived materials are utilized for mercury adsorption. However, other toxic constituents may exist in these materials, causing potential health risks. Another pathway to maximize cost-efficiency of emerging materials is reuse. Some studies have investigated the regeneration of adsorbents, and most of the emerging materials showed great potential for reuse, while other materials like MOFs and minerals cannot be regenerated while maintaining their sorption capacity (Ke et al., 2017).

It is of note that many of these adsorbents are eco-unfriendly. For instance, the synthesis of nanoparticles may use toxic reagents (e.g. $NaBH_4$), and H_2 can be formed, presenting an occupational safety risk. Besides, the large energy input during the traditional assembly procedure result in large environmental footprints (Wang et al., 2019d). During the regeneration process, eluent such as EDTA is regarded as a major contaminant in surface water (EEA, 1996; WHO, 2011). It is suggested that life cycle assessment (LCA) should be conducted to examine the overall environmental impact during the entire process of raw material acquisition, adsorbent manufacturing, regeneration and waste management (Yami et al., 2015). In addition, to quantify the overall greenhouse gas emission of these sorbents, carbon footprint analysis can be conducted (Kazemi et al., 2019). For practical use of these emerging materials, further studies should be carried out: (1) more studies should synthesis "green" sorbents to minimize the environmental impact of adsorbents; (2) more studies should focus on improving the stability of these materials, especially MOFs; (3) more research should examine the reusability of emerging materials to assure cost-efficiency; (4) more investigations about the fundamental mechanisms for mercury adsorption by these adsorbents should be conducted for a better understanding of the adsorption behavior; (5) more studies should test these materials in real conditions, rather than merely in controlled laboratory experiments.

Some innovative remediation technologies such as microbial reduction and photocatalytic nano-array lack large-scale applications, and the effectiveness of these innovative technologies in field conditions should be examined. Remediation methods involving the transformation of mercury by organisms such as phytoremediation and algae-based Hg removal can only be utilized when Hg concentrations do not exert toxic effect on organisms. Besides, the removal efficiency of mercury from the flue gas is affected by other components in the flue gas (e.g. SO_2, NO_x and H_2O). After Hg(0) oxidation, how to properly handle the oxidized Hg(II) in the fly ash is another problem. The fly ash should be stabilized to avoid Hg leaching, and feasibility of fly ash utilization for other purposes should be assessed carefully. For these innovative methods to be validated, future studies should consider following aspects: (1) the translation of experimental data to full scale operation, i.e., the industrial scale or field conditions in the case of soil remediation; (2) the combination of different remediation technologies such as combination of phytoremediation and microbial reduction to create genetically modified plants which can reduce Hg^{2+} to less toxic

Hg(0); (3) improving the separation efficiency of the adsorbents from environmental media, especially from water; (4) methods for simultaneous detection and removal of mercury from aqueous phase; (5) diminishing the impact of other constituents in the flue gas during the adsorption and oxidation process of elemental mercury.

Declaration of Competing Interest

The authors declare that they have no known competing financial interests or personal relationships that could have appeared to influence the work reported in this paper.

Acknowledgements

References

Abbas, K., Znad, H., Awual, M.R., 2018. A ligand anchored conjugate adsorbent for effective mercury(II) detection and removal from aqueous media. Chem. Eng. J. 334, 432–443.

Abraham, A.M., Kumar, S.V., Alhassan, S.M., 2018. Porous sulphur copolymer for gas-phase mercury removal and thermal insulation. Chem. Eng. J. 332, 1–7.

Aguila, B., Sun, Q., Perman, J.A., Earl, L.D., Abney, C.W., Elzein, R., Schlaf, R., Ma, S., 2017. Efficient mercury capture using functionalized porous organic polymer. Adv. Mater. 29.

Ahamad, T., Naushad, M., Al-Maswari, B.M., Ahmed, J., Alothman, Z.A., Alshehri, S.M., Alqadami, A.A., 2017. Synthesis of a recyclable mesoporous nanocomposite for efficient removal of toxic Hg^{2+} from aqueous medium. J. Ind. Eng. Chem. 53, 268–275.

Ai, K.L., Ruan, C.P., Shen, M.X., Lu, L.H., 2016. MoS_2 nanosheets with widened interlayer spacing for high-efficiency removal of mercury in aquatic systems. Adv. Funct. Mater. 26, 5542–5549.

Ali, J., Wang, H.B., Ifthikar, J., Khan, A., Wang, T., Zhan, K., Shahzad, A., Chen, Z.L., Chen, Z.Q., 2018. Efficient, stable and selective adsorption of heavy metals by thio-functionalized layered double hydroxide in diverse types of water. Chem. Eng. J. 332, 387–397.

Alijani, H., Shariatinia, Z., 2018. Synthesis of high growth rate SWCNTs and their magnetite cobalt sulfide nanohybrid as super-adsorbent for mercury removal. Chem. Eng. Res. Des. 129, 132–149.

Alimohammady, M., Jahangiri, M., Kiani, F., Tahermansouri, H., 2018. Design and evaluation of functionalized multi-walled carbon nanotubes by 3-aminopyrazole for the removal of Hg(II) and As(III) ions from aqueous solution. Res. Chem. Intermed. 44, 69–92.

AlOmar, M.K., Alsaadi, M.A., Hayyan, M., Akib, S., Ibrahim, M., Hashim, M.A., 2017. Allyl triphenyl phosphonium bromide based DES-functionalized carbon nanotubes for the removal of mercury from water. Chemosphere 167, 44–52.

Amirbahman, A., Kent, D.B., Curtis, G.P., Marvin-DiPasquale, M.C., 2013. Kinetics of homogeneous and surface-catalyzed mercury(II) reduction by iron(II). Environ. Sci. Technol. 47, 7204–7213.

Anderson, C., Moreno, F., Meech, J., 2005. A field demonstration of gold phytoextraction technology. Miner. Eng. 18, 385–392.

Anirudhan, T.S., Shainy, F., 2015. Effective removal of mercury(II) ions from chlor-alkali industrial wastewater using 2-mercaptobenzamide modified itaconic acid-grafted-magnetite nanocellulose composite. J. Colloid Interface Sci. 456, 22–31.

Attari, M., Bukhari, S.S., Kazemian, H., Rohani, S., 2017. A low-cost adsorbent from coal fly ash for mercury removal from industrial wastewater. J. Env. Chem. Eng. 5, 391–399.

Awad, F.S., Abouzeid, K.M., El-Maaty, W.M.A., El-Wakil, A.M., El-Shall, M.S., 2017. Efficient removal of heavy metals from polluted water with high selectivity for mercury(II) by 2-imino-4-thiobiuret-partially reduced graphene oxide (IT-PRGO). ACS Appl. Mater. Interfaces 9, 34230–34242.

Awual, M.R., Hasan, M.M., Eldesoky, G.E., Khaleque, M.A., Rahman, M.M., Naushad, M., 2016. Facile mercury detection and removal from aqueous media involving ligand impregnated conjugate nanomaterials. Chem. Eng. J. 290, 243–251.

Bachand, P.A.M., Kraus, T.E.C., Stumpner, E.B., Bachand, S.M., Stern, D., Liang, Y.L., Horwath, W.R., 2019. Mercury sequestration and transformation in chemically enhanced treatment wetlands. Chemosphere 217, 496–506.

Ballav, N., Das, R., Giri, S., Muliwa, A.M., Pillay, K., Maity, A., 2018. L-cysteine doped polypyrrole (PPy@L-Cyst): A super adsorbent for the rapid removal of Hg^{+2} and efficient catalytic activity of the spent adsorbent for reuse. Chem. Eng. J. 345, 621–630.

Bao, S., Li, K., Ning, P., Peng, J., Jin, X., Tang, L., 2017. Highly effective removal of mercury and lead ions from wastewater by mercaptoamine-functionalised silica-coated magnetic nano-adsorbents: Behaviours and mechanisms. Appl. Surf. Sci. 393, 457–466.

Barkay, T., Miller, S.M., Summers, A.O., 2003. Bacterial mercury resistance from atoms to

ecosystems. Fems Microbiol. Rev. 27, 355–384.

Beckers, F., Awad, Y.M., Beiyuan, J., Abrigata, J., Mothes, S., Tsang, D.C.W., Ok, Y.S., Rinklebe, J., 2019. Impact of biochar on mobilization, methylation, and ethylation of mercury under dynamic redox conditions in a contaminated floodplain soil. Environ. Int. 127, 276–290.

Beckers, F., Rinklebe, J., 2017. Cycling of mercury in the environment: Sources, fate, and human health implications: A review. Crit. Rev. Environ. Sci. Technol. 47, 693–794.

Behjati, M., Baghdadi, M., Karbassi, A., 2018. Removal of mercury from contaminated saline wasters using dithiocarbamate functionalized-magnetic nanocomposite. J. Environ. Manag. 213, 66–78.

Benoit, J.M., Gilmour, C.C., Mason, R.P., 2001. The influence of sulfide on solid phase mercury bioavailability for methylation by pure cultures of Desulfobulbus propionicus (1pr3). Environ. Sci. Technol. 35, 127–132.

Bhattacharyya, P., Reddy, K.J., 2012. Effect of flue gas treatment on the solubility and fractionation of different metals in fly ash of powder river basin coal. Water Air Soil Pollut. 223, 4169–4181.

Bhatti, A.A., Oguz, M., Yilmaz, M., 2018. One-pot synthesis of Fe_3O_4@Chitosan-pSDCalix hybrid nanomaterial for the detection and removal of Hg^{2+} ion from aqueous media. Appl. Surf. Sci. 434, 1217–1223.

Bourtsalas, A.C., Themelis, N.J., 2019. Major sources of mercury emissions to the atmosphere: The US case. Waste Manage. 85, 90–94.

Boutsika, L.G., Karapanagioti, H.K., Manariotis, I.D., 2014. Aqueous mercury sorption by biochar from malt spent rootlets. Water Air Soil Pollut. 225, 10.

Bushra, R., Naushad, M., Sharma, G., Azam, A., Alothman, Z.A., 2017. Synthesis of polyaniline based composite material and its analytical applications for the removal of highly toxic Hg^{2+} metal ion: Antibacterial activity against E. coli. Korean J. Chem. Eng. 34, 1970–1979.

Busto, Y., Cabrera, X., Tack, F.M.G., Verloo, M.G., 2011. Potential of thermal treatment for decontamination of mercury containing wastes from chlor-alkali industry. J. Hazard. Mater. 186, 114–118.

Busto, Y., Tack, F.M.G., Peralta, L.M., Cabrera, X., Arteaga-Perez, L.E., 2013. An investigation on the modelling of kinetics of thermal decomposition of hazardous mercury wastes. J. Hazard. Mater. 260, 358–367.

Chamba, I., Rosado, D., Kalinhoff, C., Thangaswamy, S., Sánchez-Rodríguez, A., Gazquez, M.J., 2017. Erato polymnioides – A novel Hg hyperaccumulator plant in ecuadorian rainforest acid soils with potential of microbe-associated phytoremediation. Chemosphere 188, 633–641.

Chavan, A.A., Pinto, J., Liakos, I., Bayer, I.S., Lauciello, S., Athanassiou, A., Fragouli, D., 2016. Spent coffee bioelastomeric composite foams for the removal of Pb^{2+} and Hg^{2+} from water. ACS Sustain. Chem. Eng. 4, 5495–5502.

Chen, C., Liu, H., Chen, T., Chen, D., Frost, R.L., 2015. An insight into the removal of Pb (II), Cu(II), Co(II), Cd(II), Zn(II), Ag(I), Hg(I), Cr(VI) by Na(I)-montmorillonite and Ca (II)-montmorillonite. Appl. Clay Sci. 118, 239–247.

Chen, D., Zhao, S., Qu, Z., Yan, N., 2018a. Cu-BTC as a novel material for elemental mercury removal from sintering gas. Fuel 217, 297–305.

Chen, G., Hai, J., Wang, H., Liu, W., Chen, F., Wang, B., 2017. Gold nanoparticles and the corresponding filter membrane as chemosensors and adsorbents for dual signal amplification detection and fast removal of mercury(II). Nanoscale 9, 3315–3321.

Chen, J., Dong, J., Chang, J., Guo, T., Yang, Q., Jia, W., Shen, S., 2018b. Characterization of an Hg(II)-volatilizing Pseudomonas sp. strain, DC-B1, and its potential for soil remediation when combined with biochar amendment. Ecotoxicol. Environ. Saf. 163, 172–179.

Chen, J., Wang, Y., Wei, X., Xu, P., Xu, W., Ni, R., Meng, J., 2018c. Magnetic solid-phase extraction for the removal of mercury from water with ternary hydrosulphonyl-based deep eutectic solvent modified magnetic graphene oxide. Talanta 188, 454–462.

Chen, S.C., Lin, W.H., Chien, C.C., Tsang, D.C.W., Kao, C.M., 2018d. Development of a two-stage biotransformation system for mercury-contaminated soil remediation. Chemosphere 200, 266–273.

Chen, W., Pei, Y., Huang, W., Qu, Z., Hu, X., Yan, N., 2016. Novel effective catalyst for elemental mercury removal from coal-fired flue gas and the mechanism investigation. Environ. Sci. Technol. 50, 2564–2572.

Chen, Y., Wu, L.H., Chen, Y.H., Bi, N., Zheng, X., Qi, H.B., Qin, M.H., Liao, X., Zhang, H.Q., Tian, Y., 2012. Determination of mercury(II) by surface-enhanced Raman scattering spectroscopy based on thiol-functionalized silver nanoparticles. Microchim. Acta 177, 341–348.

Cheng, H.B., Li, Z., Huang, Y.D., Liu, L., Wu, H.C., 2017. Pillararene-based aggregation-induced-emission-active supramolecular system for simultaneous detection and removal of mercury(II) in water. ACS Appl. Mater. Interfaces 9, 11889–11894.

Cheng, J.C., Li, Y.F., Li, L., Lu, P.P., Wang, Q., He, C.Y., 2019. Thiol-/thioether-functionalized porous organic polymers for simultaneous removal of mercury(ii) ion and aromatic pollutants in water. New J. Chem. 43, 7683–7693.

Chi, G.L., Shen, B.X., Yu, R.R., He, C., Zhang, X., 2017. Simultaneous removal of NO and Hg-0 over Ce-Cu modified V_2O_5/TiO_2 based commercial SCR catalysts. J. Hazard. Mater. 330, 83–92.

Clarkson, T.W., Magos, L., 2006. The toxicology of mercury and its chemical compounds. Crit. Rev. Toxicol. 36, 609–662.

Cote, A.P., Benin, A.I., Ockwig, N.W., O'Keeffe, M., Matzger, A.J., Yaghi, O.M., 2005. Porous, crystalline, covalent organic frameworks. Science 310, 1166–1170.

Cui, L., Guo, X., Wei, Q., Wang, Y., Gao, L., Yan, L., Yan, T., Du, B., 2015a. Removal of mercury and methylene blue from aqueous solution by xanthate functionalized magnetic graphene oxide: Sorption kinetic and uptake mechanism. J. Colloid Interface Sci. 439, 112–120.

Cui, L., Wang, Y., Gao, L., Hu, L., Yan, L., Wei, Q., Du, B., 2015b. EDTA functionalized magnetic graphene oxide for removal of Pb(II), Hg(II) and Cu(II) in water treatment: Adsorption mechanism and separation property. Chem. Eng. J. 281, 1–10.

Deliz Quiñones, K., Hovsepyan, A., Oppong-Anane, A., Bonzongo, J.C.J., 2016. Insights

into the mechanisms of mercury sorption onto aluminum based drinking water treatment residuals. J. Hazard. Mater. 307, 184–192.

Dermont, G., Bergeron, M., Mercier, G., Richer-Laflèche, M., 2008. Metal-contaminated soils: remediation practices and treatment technologies. Pract. Period. Hazard. Toxic Radioact. Waste Manage. 12, 188–209.

Devai, I., Patrick, W.H., Neue, H.U., DeLaune, R.D., Kongchum, M., Rinklebe, J., 2005. Methyl mercury and heavy metal content in soils of rivers Saale and Elbe (Germany). Anal. Lett. 38, 1037–1048.

Diagboya, P.N., Olu-Owolabi, B.I., Adebowale, K.O., 2015. Synthesis of covalently bonded graphene oxide-iron magnetic nanoparticles and the kinetics of mercury removal. RSC Adv. 5, 2536–2542.

Ding, S.Y., Wang, W., 2013. Covalent organic frameworks (COFs): from design to applications. Chem. Soc. Rev. 42, 548–568.

Duan, Y., Han, D.S., Batchelor, B., Abdel-Wahab, A., 2016. Synthesis characterization, and application of pyrite for removal of mercury. Colloids Surf., A 490, 326–335.

EEA, 1996. Requirements for Water Monitoring. European Environment Agency.

El Hanandeh, A., Abu-Zurayk, R.A., Hamadneh, I., Al-Dujaili, A.H., 2016. Characterization of biochar prepared from slow pyrolysis of Jordanian olive oil processing solid waste and adsorption efficiency of Hg^{2+} ions in aqueous solutions. Water Sci. Technol. 74, 1899–1910.

Elkhatib, E., Moharem, M., Mahdy, A., Mesalem, M., 2017. Sorption, release and forms of mercury in contaminated soils stabilized with water treatment residual nanoparticles. Land Degrad. Dev. 28, 752–761.

EPPSA, 2015. Mercury Removal Guideline for Assessment and Design Recommendations. European Power Plant Suppliers Association.

Esfandiyari, T., Nasirizadeh, N., Dehghani, M., Ehrampoosh, M.H., 2017. Graphene oxide based carbon composite as adsorbent for Hg removal: Preparation, characterization, kinetics and isotherm studies. Chin. J. Chem. Eng. 25, 1170–1175.

Essa, M.H., Mu'azu, N.D., Lukman, S., Bukhari, A., 2015. Application of box-behnken design to hybrid electrokinetic-adsorption removal of mercury from contaminated saline-sodic clay soil. Soil Sediment Contam. 24, 30–48.

Faheem, Bao, J.G., Zheng, H., Tufail, H., Irshad, S., Du, J.K., 2018. Adsorption-assisted decontamination of Hg(II) from aqueous solution by multi-functionalized corncob-derived biochar. RSC Adv. 8, 38425–38435.

Feng, S.L., Ai, Z.J., Zheng, S.M., Gu, B.H., Li, Y.C., 2014. Effects of dryout and inflow water quality on mercury methylation in a constructed wetland. Water Air Soil Pollut. 225, 11.

Fernández, S., Poschenrieder, C., Marcenò, C., Gallego, J.R., Jiménez-Gámez, D., Bueno, A., Afif, E., 2017. Phytoremediation capability of native plant species living on Pb-Zn and Hg-As mining wastes in the Cantabrian range, north of Spain. J. Geochem. Explor. 174, 10–20.

Franchi, E., Rolli, E., Marasco, R., Agazzi, G., Borin, S., Cosmina, P., Pedron, F., Rosellini, I., Barbafieri, M., Petruzzelli, G., 2017. Phytoremediation of a multi contaminated soil: mercury and arsenic phytoextraction assisted by mobilizing agent and plant growth promoting bacteria. J. Soils Sediments 17, 1224–1236.

Frohne, T., Rinklebe, J., Langer, U., Du Laing, G., Mothes, S., Wennrich, R., 2012. Biogeochemical factors affecting mercury methylation rate in two contaminated floodplain soils. Biogeosciences 9, 493–507.

Fu, W., Huang, Z., 2018. Magnetic dithiocarbamate functionalized reduced graphene oxide for the removal of Cu(II), Cd(II), Pb(II), and Hg(II) ions from aqueous solution: Synthesis, adsorption, and regeneration. Chemosphere 209, 449–456.

Gadd, G.M., 2000. Bioremedial potential of microbial mechanisms of metal mobilization and immobilization. Curr. Opin. Biotechnol. 11, 271–279.

Gao, L., Li, C.T., Li, S.H., Zhang, W., Du, X.Y., Huang, L., Zhu, Y.C., Zhai, Y.B., Zeng, G.M., 2019. Superior performance and resistance to SO2 and H2O over CoOx-modified MnOx/biomass activated carbons for simultaneous Hg-0 and NO removal. Chem. Eng. J. 371, 781–795.

Gao, L., Li, C.T., Lu, P., Zhang, J., Du, X.Y., Li, S.H., Tang, L., Chen, J.Q., Zeng, G.M., 2018. Simultaneous removal of Hg-0 and NO from simulated flue gas over columnar activated coke granules loaded with La2O3-CeO2 at low temperature. Fuel 215, 30–39.

García-Mercadoa, H.D., Fernándezb, G., Garzón-Zúñigac, M.A., Durán-Domínguez-de-Bazúaa, M.D.C., 2017. Remediation of mercury-polluted soils using artificial wetlands. Int. J. Phytoremediat. 19, 3–13.

Geng, B., Wang, H., Wu, S., Ru, J., Tong, C., Chen, Y., Liu, H., Wu, S., Liu, X., 2017. Surface-tailored nanocellulose aerogels with thiol-functional moieties for highly efficient and selective removal of Hg(II) ions from water. ACS Sustain. Chem. Eng. 5, 11715–11726.

Ghasemi, E., Heydari, A., Sillanpaa, M., 2017. Superparamagnetic Fe3O4@EDTA nanoparticles as an efficient adsorbent for simultaneous removal of Ag(I), Hg(II), Mn(II), Zn(II), Pb(II) and Cd(II) from water and soil environmental samples. Microchem. J. 131, 51–56.

Gilmour, C., Bell, T., Soren, A., Riedel, G., Riedel, G., Kopec, D., Bodaly, D., Ghosh, U., 2018. Activated carbon thin-layer placement as an in situ mercury remediation tool in a Penobscot River salt marsh. Sci. Total Environ. 621, 839–848.

Glick, B.R., 2010. Using soil bacteria to facilitate phytoremediation. Biotechnol. Adv. 28, 367–374.

Gomes, M.V.T., de Souza, R.R., Teles, V.S., Mendes, E.A., 2014. Phytoremediation of water contaminated with mercury using Typha domingensis in constructed wetland. Chemosphere 103, 228–233.

Graham, A.M., Aiken, G.R., Gilmour, C.C., 2012. Dissolved organic matter enhances microbial mercury methylation under sulfidic conditions. Environ. Sci. Technol. 46, 2715–2723.

Gunes, K., Tuncsiper, B., Masi, F., Ayaz, S., Leszczynska, D., Findik Hecan, N., Ahmad, H., 2011;6... Construction and maintenance cost analyzing of constructed wetland systems. Water Pract. Technol.

Guo, Y., Deng, J., Zhu, J., Zhou, X., Bai, R., 2016. Removal of mercury(II) and methylene blue from a wastewater environment with magnetic graphene oxide: Adsorption kinetics, isotherms and mechanism. RSC Adv. 6, 82523–82536.

Gusain, R., Kumar, N., Fosso-Kankeu, E., Ray, S.S., 2019. Efficient removal of Pb(II) and Cd(II) from industrial mine water by a hierarchical MoS2/SH-MWCNT nanocomposite. ACS Omega 4, 13922–13935.

Hadavifar, M., Bahramifar, N., Younesi, H., Rastakhiz, M., Li, Q., Yu, J., Eftekhari, E., 2016. Removal of mercury(II) and cadmium(II) ions from synthetic wastewater by a newly synthesized amino and thiolated multi-walled carbon nanotubes. J. Taiwan Inst. Chem. Eng. 67, 397–405.

Han, C., Wang, H., Xie, F., Wang, W., Zhang, T., Dreisinger, D., 2019. Feasibility study on the use of thiosulfate to remediate mercury-contaminated soil. Environ. Technol. 40, 813–821.

Hasell, T., Parker, D.J., Jones, H.A., McAllister, T., Howdle, S.M., 2016. Porous inverse vulcanised polymers for mercury capture. Chem. Commun. 52, 5383–5386.

He, C., Shen, B.X., Chi, G.L., Li, F.K., 2016. Elemental mercury removal by CeO2/TiO2-PILCs under simulated coal-fired flue gas. Chem. Eng. J. 300, 1–8.

He, F., Gao, J., Pierce, E., Strong, P.J., Wang, H., Liang, L., 2015. In situ remediation technologies for mercury-contaminated soil. Environ. Sci. Pollut. Res. 22, 8124–8147.

He, J., Reddy, G.K., Thiel, S.W., Smirniotis, P.G., Pinto, N.G., 2013. Simultaneous removal of elemental mercury and NO from flue gas using CeO2 modified MnOx/TiO2 materials. Energy Fuels 27, 4832–4839.

Henriques, B., Gonçalves, G., Emami, N., Pereira, E., Vila, M., Marques, P.A.A.P., 2016. Optimized graphene oxide foam with enhanced performance and high selectivity for mercury removal from water. J. Hazard. Mater. 301, 453–461.

Henriques, B., Rocha, L.S., Lopes, C.B., Figueira, P., Duarte, A.C., Vale, C., Pardal, M.A., Pereira, E., 2017. A macroalgae-based biotechnology for water remediation: Simultaneous removal of Cd, Pb and Hg by living Ulva lactuca. J. Environ. Manag. 191, 275–289.

Henriques, B., Rocha, L.S., Lopes, C.B., Figueira, P., Monteiro, R.J.R., Duarte, A.C., Pardal, M.A., Pereira, E., 2015. Study on bioaccumulation and biosorption of mercury by living marine macroalgae: Prospecting for a new remediation biotechnology applied to saline waters. Chem. Eng. J. 281, 759–770.

Hsu-Kim, H., Kucharzyk, K.H., Zhang, T., Deshusses, M.A., 2013. Mechanisms regulating mercury bioavailability for methylating microorganisms in the aquatic environment: a critical review. Environ. Sci. Technol. 47, 2441–2456.

Hua, Y.M., Heal, K.V., Friesl-Hanl, W., 2017. The use of red mud as an immobiliser for metal/metalloid-contaminated soil: A review. J. Hazard. Mater. 325, 17–30.

Huang, L., He, M., Chen, B., Hu, B., 2015a. A designable magnetic MOF composite and facile coordination-based post-synthetic strategy for the enhanced removal of $Hg < sup > 2+ < /sup >$ from water. J. Mater. Chem. 3, 11587–11595.

Huang, L., He, M., Chen, B., Hu, B., 2016. A mercapto functionalized magnetic Zr-MOF by solvent-assisted ligand exchange for Hg^{2+} removal from water. J. Mater. Chem. 4, 5159–5166.

Huang, L., He, M., Chen, B.B., Cheng, Q., Hu, B., 2017a. Highly efficient magnetic nitrogen-doped porous carbon prepared by one-step carbonization strategy for Hg^{2+} removal from water. ACS Appl. Mater. Interfaces 9, 2550–2559.

Huang, L.J., He, M., Chen, B.B., Hu, B., 2015b. A designable magnetic MOF composite and facile coordination-based post-synthetic strategy for the enhanced removal of Hg^{2+} from water. J. Mater. Chem. 3, 11587–11595.

Huang, N., Zhai, L., Xu, H., Jiang, D., 2017b. Stable covalent organic frameworks for exceptional mercury removal from aqueous solutions. J. Am. Chem. Soc. 139, 2428–2434.

Huang, Y., Gong, Y., Tang, J., Xia, S., 2019a. Effective removal of inorganic mercury and methylmercury from aqueous solution using novel thiol-functionalized graphene oxide/Fe-Mn composite. J. Hazard. Mater. 130–139.

Huang, Y., Xia, S., Lyu, J., Tang, J., 2019b. Highly efficient removal of aqueous Hg^{2+} and CH_3Hg^+ by selective modification of biochar with 3-mercaptopropyltrimethoxysilane. Chem. Eng. J. 360, 1646–1655.

Hummers, W.S., Offeman, R.E., 1958. Preparation of graphtic oxide. J. Am. Chem. Soc. 80 1339 1339.

Hung, P.C., Chang, S.H., Ou-Yang, C.C., Chang, M.B., 2016. Simultaneous removal of PCDD/Fs, pentachlorophenol and mercury from contaminated soil. Chemosphere 144, 50–58.

Jampaiah, D., Ippolito, S.J., Sabri, Y.M., Reddy, B.M., Bhargava, S.K., 2015. Highly efficient nanosized Mn and Fe codoped ceria-based solid solutions for elemental mercury removal at low flue gas temperatures. Catal. Sci. Technol. 5, 2913–2924.

Jia, X., O'Connor, D., Hou, D., Jin, Y., Li, G., Zheng, C., Ok, Y.S., Tsang, D.C.W., Luo, J., 2019. Groundwater depletion and contamination: Spatial distribution of groundwater resources sustainability in China. Sci. Total Environ. 672, 551–562.

Jiang, W., Xiantuo, C., Chaoen, L., Yongfeng, Q., Xuemei, Q., Jianxing, R., Binxia, Y., Bu, N., Ruixing, Z., Jing, Z., Tianfang, H., 2016. Hydrothermal synthesis of carbon spheres - BiOI/BiOIO3 heterojunctions for photocatalytic removal of gaseous Hg-0 under visible light. Chem. Eng. J. 304, 533–543.

Johs, A., Eller, V.A., Mehlhorn, T.L., Brooks, S.C., Harper, D.P., Mayes, M.A., Pierce, E.M., Peterson, M.J., 2019. Dissolved organic matter reduces the effectiveness of sorbents for mercury removal. Sci. Total Environ. 690, 410–416.

Kabiri, S., Tran, D.N.H., Azari, S., Losic, D., 2015. Graphene-diatom silica aerogels for efficient removal of mercury ions from water. ACS Appl. Mater. Interfaces 7, 11815–11823.

Kakareka, S.V., Kukharchyk, T.I., 2012. Trends of mercury emissions from the Chlor-Alkali industry in EECCA. Int. J. Environ. Sci. (India) 2, 1585–1595.

Kandjani, A.E., Sabri, Y.M., Mohammad-Taheri, M., Bansal, V., Bhargava, S.K., 2015. Detect, remove and reuse: A new paradigm in sensing and removal of Hg (II) from wastewater via SERS-active ZnO/Ag nanoarrays. Environ. Sci. Technol. 49,

1578–1584.

Karmakar, M., Mondal, H., Mahapatra, M., Chattopadhyay, P.K., Chatterjee, S., Singha, N.R., 2019. Pectin-grafted terpolymer superadsorbent via N-H activated strategic protrusion of monomer for removals of Cd(II), Hg(II), and Pb(II). Carbohydr. Polym. 206, 778–791.

Kazemi, A., Bahramifar, N., Heydari, A., Olsen, S.I., 2019. Synthesis and sustainable assessment of thiol-functionalization of magnetic graphene oxide and superparamagnetic Fe3O4@SiO2 for Hg(II) removal from aqueous solution and petrochemical wastewater. J. Taiwan Inst. Chem. Eng. 95, 78–93.

Kazemi, F., Younesi, H., Ghoreyshi, A.A., Bahramifar, N., Heidari, A., 2016. Thiol-incorporated activated carbon derived from fir wood sawdust as an efficient adsorbent for the removal of mercury ion: Batch and fixed-bed column studies. Process Saf. Environ. Prot. 100, 22–35.

Ke, F., Jiang, J., Li, Y.Z., Liang, J., Wan, X.C., Ko, S., 2017. Highly selective removal of Hg^{2+} and Pb^{2+} by thiol-functionalized Fe3O4@metal-organic framework core-shell magnetic microspheres. Appl. Surf. Sci. 413, 266–274.

Kenawy, I.M.M., Abou El-Reash, Y.G., Hassanien, M.M., Alnagar, N.R., Mortada, W.I., 2018. Use of microwave irradiation for modification of mesoporous silica nanoparticles by thioglycolic acid for removal of cadmium and mercury. Micropor. Mesopor. Mater. 258, 217–227.

Khan, F.I., Husain, T., Hejazi, R., 2004. An overview and analysis of site remediation technologies. J. Environ. Manag. 71, 95–122.

Krzyzynska, R., Hutson, N.D., Zhao, Y., Szeliga, Z., Regucki, P., 2018. Mercury removal and its fate in oxidant enhanced wet flue gas desulphurization slurry. Fuel 211, 876–882.

Kumar, N., Fosso-Kankeu, E., Ray, S.S., 2019. Achieving controllable MoS2 nanostructures with increased interlayer spacing for efficient removal of Pb(II) from aquatic systems. ACS Appl. Mater. Interfaces 11, 19141–19155.

Kyzas, G.Z., Kostoglou, M., 2015. Swelling-adsorption interactions during mercury and nickel ions removal by chitosan derivatives. Sep. Purif. Technol. 149, 92–102.

Lee, W.R., Eom, Y., Lee, T.G., 2017. Mercury recovery from mercury-containing wastes using a vacuum thermal desorption system. Waste Manage. 60, 546–551.

Lei, P., Nunes, L.M., Liu, Y.R., Zhong, H., Pan, K., 2019. Mechanisms of algal biomass input enhanced microbial Hg methylation in lake sediments. Environ. Int. 126, 279–288.

Leus, K., Folens, K., Nicomel, N.R., Perez, J.P.H., Filippousi, M., Meledina, M., Dirtu, M.M., Turner, S., Van Tendeloo, G., Garcia, Y., Du Laing, G., Van Der Voort, P., 2018. Removal of arsenic and mercury species from water by covalent triazine framework encapsulated γ-Fe2O3 nanoparticles. J. Hazard. Mater. 353, 312–319.

Leus, K., Perez, J.P.H., Folens, K., Meledina, M., Van Tendeloo, G., Du Laing, G., Van Der Voort, P., 2017. UiO-66-(SH)(2) as stable, selective and regenerable adsorbent for the removal of mercury from water under environmentally-relevant conditions. Faraday Discuss. 201, 145–161.

Leven, A., Vlassopoulos, D., Kanematsu, M., Goin, J., O'Day, P.A., 2018. Characterization of manganese oxide amendments for in situ remediation of mercury-contaminated sediments. Environ. Sci. Process. Impacts 20, 1761–1773.

Lewis, A.S., Huntington, T.G., Marvin-Dipasquale, M.C., Amirbahman, A., 2016. Mercury remediation in wetland sediment using zero-valent iron and granular activated carbon. Environ. Pollut. 212, 366–373.

Li, G., Shen, B., Li, F., Tian, L., Singh, S., Wang, F., 2015a. Elemental mercury removal using biochar pyrolyzed from municipal solid waste. Fuel Process. Technol. 133, 43–50.

Li, G., Shen, B., Li, Y., Zhao, B., Wang, F., He, C., Wang, Y., Zhang, M., 2015b. Removal of element mercury by medicine residue derived biochars in presence of various gas compositions. J. Hazard. Mater. 298, 162–169.

Li, G., Shen, B., Lu, F., 2015c. The mechanism of sulfur component in pyrolyzed char from waste tire on the elemental mercury removal. Chem. Eng. J. 273, 446–454.

Li, G., Shen, B., Wang, Y., Yue, S., Xi, Y., An, M., Ren, K., 2015d. Comparative study of element mercury removal by three bio-chars from various solid wastes. Fuel 145, 189–195.

Li, H., Liu, H., Zhang, J., Cheng, Y., Zhang, C., Fei, X., Xian, Y., 2017. Platinum nanoparticle encapsulated metal-organic frameworks for colorimetric measurement and facile removal of mercury(II). ACS Appl. Mater. Interfaces 9, 40716–40725.

Li, H., Zhu, L., Wang, J., Li, L., Shih, K., 2016. Development of nano-sulfide sorbent for efficient removal of elemental mercury from coal combustion fuel gas. Environ. Sci. Technol. 50, 9551–9557.

Li, X., Lee, J.Y, Heald, S., 2012. XAFS characterization of mercury captured on cupric chloride-impregnated sorbents. Fuel 93, 618–624.

Li, X.S., Huang, Q., Luo, C., Zhou, D., Xu, Y.Q., Zhang, L.Q., Zheng, C.G., 2018. Effect of acid gases on elemental mercury removal in an oxy-fuel CO2 compression process. Energy Fuels 32, 4334–4340.

Liang, L., Chen, Q., Jiang, F., Yuan, D., Qian, J., Lv, G., Xue, H., Liu, L., Jiang, H.L., Hong, M., 2016. In situ large-scale construction of sulfur-functionalized metal-organic framework and its efficient removal of Hg(II) from water. J. Mater. Chem. 4, 15370–15374.

Liang, L.F., Liu, L.Y., Jiang, F.L., Liu, C.P., Yuan, D.Q., Chen, Q.H., Wu, D., Jiang, H.L., Hong, M.C., 2018. Incorporation of In2S3 nanoparticles into a metal-organic framework for ultrafast removal of hg from water. Inorg. Chem. 57, 4891–4897.

Lin, Q., Mao, P.P., Fan, Y.Q., Liu, L., Liu, J., Zhang, Y.M., Yao, H., Wei, T.B., 2017. A novel supramolecular polymer gel based on naphthalimide functionalized-pillar[5]arene for the fluorescence detection of Hg^{2+} and I-and recyclable removal of Hg^{2+} via cation-π interactions. Soft Matter 13, 7085–7089.

Linacre, N.A., Whiting, S.N., Angle, J.S., 2005. The impact of uncertainty on phytoremediation project costs. Int. J. Phytoremediat. 7, 259–269.

Liu, H., Zhao, Y., Zhou, Y., Chang, L., Zhang, J., 2019a. Removal of gaseous elemental mercury by modified diatomite. Sci. Total Environ. 652, 651–659.

Liu, J., Guo, R.T., Guan, Z.Z., Sun, X., Pan, W.G., Liu, X.Y., Wang, Z.Y., Shi, X., Qin, H., Qiu, Z.Z., Liu, S.W., 2019b. Simultaneous removal of NO and Hg-0 over Nb-Modified MnTiOx catalyst. Int. J. Hydrogen Energy 44, 835–843.

Liu, P., Ptacek, C.J., Blowes, D.W., Landis, R.C., 2016. Mechanisms of mercury removal by biochars produced from different feedstocks determined using X-ray absorption spectroscopy. J. Hazard. Mater. 308, 233–242.

Liu, Y., Wang, X., Wu, H., 2017. Reusable DNA-functionalized-graphene for ultrasensitive mercury (II) detection and removal. Biosens. Bioelectron. 87, 129–135.

Liu, Y., Wang, Y., 2018. Elemental mercury removal from flue gas using heat and Co^{2+}/Fe^{2+} coactivated oxone oxidation system. Chem. Eng. J. 348, 464–475.

Liu, Y., Wang, Y., Wang, Q., Pan, J., Zhang, Y., Zhou, J., Zhang, J., 2015. A study on removal of elemental mercury in flue gas using fenton solution. J. Hazard. Mater. 292, 164–172.

Liu, Y., Wang, Y.J., Wang, H.Q., Wu, Z.B., 2011. Catalytic oxidation of gas-phase mercury over Co/TiO2 catalysts prepared by sol-gel method. Catal. Commun. 12, 1291–1294.

Liu, Y.X., Adewuyi, Y.G., 2016. A review on removal of elemental mercury from flue gas using advanced oxidation process: Chemistry and process. Chem. Eng. Res. Des. 112, 199–250.

Liu, Y.X., Wang, Y., 2019. Gaseous elemental mercury removal using VUV and heat coactivation of Oxone/H2O/O2 in a VUV-spraying reactor. Fuel 243, 352–361.

Liu, Z., Wang, L.A., Ding, S., Xiao, H., 2018a. Enhancer assisted-phytoremediation of mercury-contaminated soils by Oxalis corniculata L., and rhizosphere microorganism distribution of Oxalis corniculata L. Ecotoxicol. Environ. Saf. 160, 171–177.

Liu, Z., Yang, W., Xu, W., Liu, Y., 2018b. Removal of elemental mercury by bio-chars derived from seaweed impregnated with potassium iodine. Chem. Eng. J. 339, 468–478.

Luo, F., Chen, J.L., Dang, L.L., Zhou, W.N., Lin, H.L., Li, J.Q., Liu, S.J., Luo, M.B., 2015. High-performance Hg^{2+} removal from ultra-low-concentration aqueous solution using both acylamide- and hydroxyl-functionalized metal-organic framework. J. Mater. Chem. 3, 9616–9620.

Lv, S., Yang, B., Kou, Y., Zeng, J., Wang, R., Xiao, Y., Li, F., Lu, Y., Mu, Y., Zhao, C., 2018. Assessing the difference of tolerance and phytoremediation potential in mercury contaminated soil of a non-food energy crop, Helianthus tuberosus L (Jerusalem artichoke). PeerJ.

Ma, F., Peng, C., Hou, D., Wu, B., Zhang, Q., Li, F., Gu, Q., 2015. Citric acid facilitated thermal treatment: An innovative method for the remediation of mercury contaminated soil. J. Hazard. Mater. 300, 546–552.

Ma, F.J., Zhang, Q., Xu, D.P., Hou, D.Y., Li, F.S., Gu, Q.B., 2014. Mercury removal from contaminated soil by thermal treatment with FeCl3 at reduced temperature. Chemosphere 117, 388–393.

Ma, L.J., Islam, S.M., Xiao, C.L., Zhao, J., Liu, H.Y., Yuan, M.W., Sun, G.B., Li, H.F., Ma, S.L., Kanatzidis, M.G., 2017a. Rapid simultaneous removal of toxic anions [H5eO3−], [SeO3 2−], and [SeO4 2−], and metals Hg2+, Cu2+, and Cd2+ by MoS4 2− intercalated layered double hydroxide. J. Am. Chem. Soc. 139, 12745–12757.

Ma, L.J., Wang, Q., Islam, S.M., Liu, Y.C., Ma, S.L., Kanatzidis, M.G., 2016. Highly selective and efficient removal of heavy metals by layered double hydroxide intercalated with the MoS4 2− ion. J. Am. Chem. Soc. 138, 2858–2866.

Ma, Y., Zhang, D., Sun, H., Wu, J., Liang, P., Zhang, H., 2018. Fe-Ce mixed oxides supported on carbon nanotubes for simultaneous removal of NO and Hg-0 in flue gas. Ind. Eng. Chem. Res. 57, 3187–3194.

Ma, Y.P., Mu, B.L., Yuan, D.L., Zhang, H.Z., Xu, H.M., 2017b. Design of MnO2/CeO2-MnO2 hierarchical binary oxides for elemental mercury removal from coal-fired flue gas. J. Hazard. Mater. 333, 186–193.

Mahbub, K.R., Krishnan, K., Megharaj, M., Naidu, R., 2016. Bioremediation potential of a highly mercury resistant bacterial strain Sphingobium SA2 isolated from contaminated soil. Chemosphere 144, 330–337.

Mahbub, K.R., Krishnan, K., Naidu, R., Megharaj, M., 2017. Mercury remediation potential of a mercury resistant strain Sphingopyxis sp. SE2 isolated from contaminated soil. J. Environ. Sci. (China) 51, 128–137.

Maia, L.F.O., Hott, R.C., Ladeira, P.C.C., Batista, B.L., Andrade, T.G., Santos, M.S., Faria, M.C.S., Oliveira, L.C.A., Monteiro, D.S., Pereira, M.C., Rodrigues, J.L., 2019. Simple synthesis and characterization of L-Cystine functionalized delta-FeOOH for highly efficient Hg(II) removal from contamined water and mining waste. Chemosphere 215, 422–431.

Manna, B., Raj, C.R., 2018. Nanostructured sulfur-doped porous reduced graphene oxide for the ultrasensitive electrochemical detection and efficient removal of Hg(II). ACS Sustainable Chem. Eng. 6, 6175–6182.

Marcano, D.C., Kosynkin, D.V., Berlin, J.M., Sinitskii, A., Sun, Z.Z., Slesarev, A., Alemany, L.B., Lu, W., Tour, J.M., 2010. Improved synthesis of graphene oxide. ACS Nano 4, 4806–4814.

Marczak, M., Budzyń, S., Szczurowski, J., Kogut, K., Burmistrz, P., 2019. Active methods of mercury removal from flue gases. Environ. Sci. Pollut. Res. 26, 8383–8392.

Marrugo-Negrete, J., Durango-Hernández, J., Pinedo-Hernández, J., Olivero-Verbel, J., Díez, S., 2015. Phytoremediation of mercury-contaminated soils by Jatropha curcas. Chemosphere 127, 58–63.

Marrugo-Negrete, J., Enamorado-Montes, G., Durango-Hernández, J., Pinedo-Hernández, J., Díez, S., 2017. Removal of mercury from gold mine effluents using Limnocharis flava in constructed wetlands. Chemosphere 167, 188–192.

Marrugo-Negrete, J., Marrugo-Madrid, S., Pinedo-Hernández, J., Durango-Hernández, J., Díez, S., 2016. Screening of native plant species for phytoremediation potential at a Hg-contaminated mining site. Sci. Total Environ. 542, 809–816.

Mathema, V.B., Thakuri, B.C., Sillanpaa, M., 2011. Bacterial mer operon-mediated detoxification of mercurial compounds: a short review. Arch. Microbiol. 193, 837–844.

McCarthy, D., Edwards, G.C., Gustin, M.S., Care, A., Miller, M.B., Sunna, A., 2017. An innovative approach to bioremediation of mercury contaminated soils from industrial mining operations. Chemosphere 184, 694–699.

Merí-Bofí, L., Royuela, S., Zamora, F., Ruiz-González, M.L., Segura, J.L., Muñoz-Olivas, R., Mancheño, M.J., 2017. Thiol grafted imine-based covalent organic frameworks for water remediation through selective removal of Hg(II). J. Mater. Chem. 5, 17973–17981.

Moghaddam, H.K., Pakizeh, M., 2015. Experimental study on mercury ions removal from aqueous solution by MnO$_2$/CNTs nanocomposite adsorbent. J. Ind. Eng. Chem. 21, 221–229.

Moharem, M., Elkhatib, E., Mesalem, M., 2019. Remediation of chromium and mercury polluted calcareous soils using nanoparticles: Sorption –desorption kinetics, speciation and fractionation. Environ. Res. 366–373.

Molina, J.A., Oyarzun, R., Esbri, J.M., Higueras, P., 2006. Mercury accumulation in soils and plants in the Almaden mining district, Spain: one of the most contaminated sites on Earth. Environ. Geochem. Health 28, 487–498.

Mon, M., Lloret, F., Ferrando-Soria, J., Martí-Gastaldo, C., Armentano, D., Pardo, E., 2016. Selective and efficient removal of mercury from aqueous media with the highly flexible arms of a BioMOF. Angew. Chem., Int. Ed. 55, 11167–11172.

Mondal, H., Karmakar, M., Chattopadhyay, P.K., Singha, N.R., 2019a. Starch-g-tetrapolymer hydrogel via in situ attached monomers for removals of Bi(III) and/or Hg(II) and dye(s): RSM-based optimization. Carbohydr. Polym. 213, 428–440.

Mondal, S., Chatterjee, S., Mondal, S., Bhaumik, A., 2019b. Thioether-functionalized covalent triazine nanospheres: a robust adsorbent for mercury removal. ACS Sustainable Chem. Eng. 7, 7353–7361.

Mu'azu, N.D., Usman, A., Jarrah, N., Alagha, O., 2016. Pulsed electrokinetic removal of chromium, mercury and cadmium from contaminated mixed clay soils. Soil Sediment Contam. 25, 757–775.

Muller, K.A., Brooks, S.C., 2019. Effectiveness of sorbents to reduce mercury methylation. Environ. Eng. Sci. 36, 361–371.

Mulligan, C.N., Yong, R.N., Gibbs, B.F., 2001. Remediation technologies for metal-contaminated soils and groundwater: an evaluation. Eng. Geol. 60, 193–207.

Nascimento, A.M.A., Chartone-Souza, E., 2003. Operon mer: bacterial resistance to mercury and potential for bioremediation of contaminated environments. Genetics and molecular research: GMR 2, 92–101.

Nasirimoghaddam, S., Zeinali, S., Sabbaghi, S., 2015. Chitosan coated magnetic nanoparticles as nano-adsorbent for efficient removal of mercury contents from industrial aqueous and oily samples. J. Ind. Eng. Chem. 27, 79–87.

Novoselov, K.S., Geim, A.K., Morozov, S.V., Jiang, D., Zhang, Y., Dubonos, S.V., Grigorieva, I.V., Firsov, A.A., 2004. Electric field effect in atomically thin carbon films. Science 306, 666–669.

O'Connor, D., Hou, D.Y., Ok, Y.S., Mulder, J., Duan, L., Wu, Q.R., Wang, S.X., Tack, F.M.G., Rinklebe, J., 2019. Mercury speciation, transformation, and transportation in soils, atmospheric flux, and implications for risk management: A critical review. Environ. Int. 126, 747–761.

O'Connor, D., Peng, T., Li, G., Wang, S., Duan, L., Mulder, J., Cornelissen, G., Cheng, Z., Yang, S., Hou, D., 2018. Sulfur-modified rice husk biochar: A green method for the remediation of mercury contaminated soil. Sci. Total Environ. 621, 819–826.

Parker, D.J., Jones, H.A., Petcher, S., Cervini, L., Griffin, J.M., Akhtar, R., Hasell, T., 2017. Low cost and renewable sulfur-polymers by inverse vulcanisation, and their potential for mercury capture. J. Mater. Chem. 5, 11682–11692.

Pehnec, G., Sisovic, A., Vadjic, V., Zuzul, S., 2010. Influence of waste dump remediation on the levels of mercury in the air. Bull. Environ. Contam. Toxicol. 84, 623–627.

Peng, R.X., Chen, G., Zhou, F., Man, R.L., Huang, J.H., 2019. Catalyst-free synthesis of triazine-based porous organic polymers for Hg2+ adsorptive removal from aqueous solution. Chem. Eng. J. 371, 260–266.

Piao, H.S., Bishop, P.L., 2006. Stabilization of mercury-containing wastes using sulfide. Environ. Pollut. 139, 498–506.

Pirrone, N., Cinnirella, S., Feng, X., Finkelman, R.B., Friedli, H.R., Leaner, J., Mason, R., Mukherjee, A.B., Stracher, G.B., Streets, D.G., Telmer, K., 2010. Global mercury emissions to the atmosphere from anthropogenic and natural sources. Atmos. Chem. Phys. 10, 5951–5964.

Qi, X.M., Gu, M.L., Zhu, X.Y., Wu, J., Long, H.M., He, K., Wu, Q., 2016. Fabrication of BiOIO$_3$ nanosheets with remarkable photocatalytic oxidation removal for gaseous elemental mercury. Chem. Eng. J. 285, 11–19.

Qu, Z., Fang, L., Chen, D., Xu, H., Yan, N., 2017. Effective and regenerable Ag/graphene adsorbent for Hg(II) removal from aqueous solution. Fuel 203, 128–134.

Quinones, M.A., Ruiz-Diez, B., Fajardo, S., Lopez-Berdonces, M.A., Higueras, P.L., Fernandez-Pascual, M., 2013. Lupinus albus plants acquire mercury tolerance when inoculated with an Hg-resistant Bradyrhizobium strain. Plant Physiol. Biochem. 73, 168–175.

Ram, B., Chauhan, G.S., 2018. New spherical nanocellulose and thiol-based adsorbent for rapid and selective removal of mercuric ions. Chem. Eng. J. 331, 587–596.

Rascio, N., Navari-Izzo, F., 2011. Heavy metal hyperaccumulating plants: How and why do they do it? And what makes them so interesting? Plant Sci. 180, 169–181.

Reddy, G.K., He, J., Thiel, S.W., Pinto, N.G., Smirniotis, P.G., 2015. Sulfur-tolerant Mn-Ce-Ti sorbents for elemental mercury removal from flue gas: Mechanistic investigation by XPS. J. Phys. Chem. 119, 8634–8644.

Robles, I., Lozano, M.J., Solís, S., Hernández, G., Paz, M.V., Olvera, M.G., Bustos, E., 2015. Electrokinetic treatment of mercury-polluted soil facilitated by ethylenediaminetetraacetic acid coupled with a reactor with a permeable reactive barrier of iron to recover mercury (II) from water. Electrochim. Acta 181, 68–72.

Rocha, L.S., Almeida, Â., Nunes, C., Henriques, B., Coimbra, M.A., Lopes, C.B., Silva, C.M., Duarte, A.C., Pereira, E., 2016. Simple and effective chitosan based films for the removal of Hg from waters: Equilibrium, kinetic and ionic competition. Chem. Eng. J. 300, 217–229.

Rodriguez, O., Padilla, I., Tayibi, H., Lopez-Delgado, A., 2012. Concerns on liquid mercury and mercury-containing wastes: A review of the treatment technologies for the safe storage. J. Environ. Manag. 101, 197–205.

Romera, E., Gonzalez, F., Ballester, A., Blazquez, M.L., Munoz, J.A., 2007. Comparative study of biosorption of heavy metals using different types of algae. Bioresour. Technol. 98, 3344–3353.

Rosestolato, D., Bagatin, R., Ferro, S., 2015. Electrokinetic remediation of soils polluted by heavy metals (mercury in particular). Chem. Eng. J. 264, 16–23.

Sajjadi, S.A., Mohammadzadeh, A., Tran, H.N., Anastopoulos, I., Dotto, G.L., Lopičić, Z.R., Sivamani, S., Rahmani-Sani, A., Ivanets, A., Hosseini-Bandegharaei, A., 2018. Efficient mercury removal from wastewater by pistachio wood wastes-derived activated carbon prepared by chemical activation using a novel activating agent. J. Environ. Manag. 223, 1001–1009.

Saleh, T.A., Tuzen, M., Sarı, A., 2018. Polyamide magnetic palygorskite for the simultaneous removal of Hg(II) and methyl mercury; with factorial design analysis. J. Environ. Manag. 211, 323–333.

Saraydin, D., Yildirim, E.S., Karadag, E., Guven, O., 2018. Radiation-synthesized acrylamide/crotonic acid hydrogels for selective mercury (II) ion adsorption. Adv. Polym. Technol. 37, 8.

Scala, F., Cimino, S., 2015. Elemental mercury capture and oxidation by a regenerable manganese-based sorbent: The effect of gas composition. Chem. Eng. J. 278, 134–139.

Selin, N.E., 2009. Global biogeochemical cycling of mercury: a review. Annu. Rev. Environ. Resour. 34, 43–63.

Shafiabadi, M., Dashti, A., Tayebi, H.A., 2016. Removal of Hg (II) from aqueous solution using polypyrrole/SBA-15 nanocomposite: Experimental and modeling. Synth. Met. 212, 154–160.

Shan, C., Ma, Z.Y., Tong, M.P., Ni, J.R., 2015. Removal of Hg(II) by poly(1-vinylimidazole)-grafted Fe$_3$O$_4$@SiO$_2$ magnetic nanoparticles. Water Res. 69, 252–260.

Shao, H., Liu, X., Zhou, Z., Zhao, B., Chen, Z., Xu, M., 2016. Elemental mercury removal using a novel KI modified bentonite supported by starch sorbent. Chem. Eng. J. 291, 306–316.

Shen, B., Li, G., Wang, F., Wang, Y., He, C., Zhang, M., Singh, S., 2015. Elemental mercury removal by the modified bio-char from medicinal residues. Chem. Eng. J. 272, 28–37.

Shen, B., Tian, L., Li, F., Zhang, X., Xu, H., Singh, S., 2017. Elemental mercury removal by the modified bio-char from waste tea. Fuel 187, 189–196.

Shirzadi, H., Nezamzadeh-Ejhieh, A., 2017. An efficient modified zeolite for simultaneous removal of Pb(II) and Hg(II) from aqueous solution. J. Mol. Liq. 230, 221–229.

Sierra, M.J., Millán, R., López, F.A., Alguacil, F.J., Cañadas, I., 2016. Sustainable remediation of mercury contaminated soils by thermal desorption. Environ. Sci. Pollut. Res. 23, 4898–4907.

Singha Deb, A.K., Dwivedi, V., Dasgupta, K., Musharaf Ali, S., Shenoy, K.T., 2017. Novel amidoamine functionalized multi-walled carbon nanotubes for removal of mercury (II) ions from wastewater: Combined experimental and density functional theoretical approach. Chem. Eng. J. 313, 899–911.

Song, Y.H., Lu, M.C., Huang, B., Wang, D.L., Wang, G., Zhou, L., 2018. Decoration of defective MoS$_2$ nanosheets with Fe$_3$O$_4$ nanoparticles as superior magnetic adsorbent for highly selective and efficient mercury ions (Hg^{2+}) removal. J. Alloys Compd. 737, 113–121.

Song, Y.P., Sun, Q., Aguila, B., Ma, S.Q., 2019. Opportunities of covalent organic frameworks for advanced applications. Adv. Sci. 6, 34.

Subrahmanyam, K.S., Malliakas, C.D., Sarma, D., Armatas, G.S., Wu, J., Kanatzidis, M.G., 2015. Ion-Exchangeable molybdenum sulfide porous chalcogel: gas adsorption and capture of iodine and mercury. J. Am. Chem. Soc. 137, 13943–13948.

Sun, Q., Aguila, B., Perman, J., Earl, L.D., Abney, C.W., Cheng, Y., Wei, H., Nguyen, N., Wojtas, L., Ma, S., 2017. Postsynthetically modified covalent organic frameworks for efficient and effective mercury removal. J. Am. Chem. Soc. 139, 2786–2793.

Sun, Y., Liu, Y., Lou, Z., Yang, K., Lv, D., Zhou, J., Baig, S.A., Xu, X., 2018. Enhanced performance for Hg(II) removal using biomaterial (CMC/gelatin/starch) stabilized FeS nanoparticles: Stabilization effects and removal mechanism. Chem. Eng. J. 344, 616–624.

Tack, F.M.G., Rinklebe, J., Ok, Y.S., 2019. Interactions between biochar and trace elements in the environment. Sci. Total Environ. 649, 792.

Tadjarodi, A., Moazen Ferdowsi, S., Zare-Dorabei, R., Barzin, A., 2016. Highly efficient ultrasonic-assisted removal of Hg(II) ions on graphene oxide modified with 2-pyridinecarboxaldehyde thiosemicarbazone: Adsorption isotherms and kinetics studies. Ultrason. Sonochem. 33, 118–128.

Tang, J., Huang, Y., Gong, Y., Lyu, H., Wang, Q., Ma, J., 2016. Preparation of a novel graphene oxide/Fe-Mn composite and its application for aqueous Hg(II) removal. J. Hazard. Mater. 316, 151–158.

Tang, J., Lv, H., Gong, Y., Huang, Y., 2015. Preparation and characterization of a novel graphene/biochar composite for aqueous phenanthrene and mercury removal. Bioresour. Technol. 196, 355–363.

Tran, L., Wu, P., Zhu, Y., Yang, L., Zhu, N., 2015. Highly enhanced adsorption for the removal of Hg(II) from aqueous solution by Mercaptoethylamine/Mercaptopropyltrimethoxysilane functionalized vermiculites. J. Colloid Interface Sci. 445, 348–356.

UNEP, 2018. Global Mercury Assessment. United Nations Environment Programme, Geneva.

USEPA, 2000. Constructed Wetlands Treatment of Municipal Wastewater. EPA 625/R-99/010. United States Environmental Protection Agency.

USEPA, 2000. Introduction to phytoremediation. U.S. EPA Report EPA/600/R-99/107. United States Environmental Protection Agency.

USEPA, 2007. Treatment Technologies for Mercury in Soil, Waste and Water, EPA-542-R-07-003. United States Environmental Protection Agency.

USEPA, 2017. Superfund Remedy Report (15th edition). United States Environmental Protection Agency.

Venkateswarlu, S., Yoon, M., 2015. Surfactant-free green synthesis of Fe$_3$O$_4$ nanoparticles capped with 3,4-dihydroxy-phenethylcarbamodithioate: stable recyclable magnetic

nanoparticles for the rapid and efficient removal of Hg(II) ions from water. Dalton Trans. 44, 18427–18437.

Vlassopoulos, D., Kanematsu, M., Henry, E.A., Goin, J., Leven, A., Glaser, D., Brown, S.S., O'Day, P.A., 2018. Manganese(iv) oxide amendments reduce methylmercury concentrations in sediment porewater. Environ. Sci. Process. Impacts 20, 1746–1760.

Wagner-Dobler, I., 2003. Pilot plant for bioremediation of mercury-containing industrial wastewater. Appl. Microbiol. Biotechnol. 62, 124–133.

Wan, X., Lei, M., Chen, T., 2016. Cost–benefit calculation of phytoremediation technology for heavy-metal-contaminated soil. Sci. Total Environ. 563–564, 796–802.

Wang, F.Y., Wang, S.X., Zhang, L., Yang, H., Gao, W., Wu, Q.R., Hao, J.M., 2016a. Mercury mass flow in iron and steel production process and its implications for mercury emission control. J. Environ. Sci. 43, 293–301.

Wang, F.Y., Wang, S.X., Zhang, L., Yang, H., Wu, Q.R., Hao, J.M., 2016b. Characteristics of mercury cycling in the cement production process. J. Hazard. Mater. 302, 27–35.

Wang, H., Liu, Y., Ifthikar, J., Shi, L., Khan, A., Chen, Z., Chen, Z., 2018a. Towards a better understanding on mercury adsorption by magnetic bio-adsorbents with γ-Fe$_2$O$_3$ from pinewood sawdust derived hydrochar: Influence of atmosphere in heat treatment. Bioresour. Technol. 256, 269–276.

Wang, J., Shaheen, S.M., Swertz, A.-C., Rennert, T., Feng, X., Rinklebe, J., 2019a. Sulfur-modified organoclay promotes plant uptake and affects geochemical fractionation of mercury in a polluted floodplain soil. J. Hazard. Mater. 371, 687–693.

Wang, J.X., Feng, X.B., Anderson, C.W.N., Xing, Y., Shang, L.H., 2012. Remediation of mercury contaminated sites - A review. J. Hazard. Mater. 221, 1–18.

Wang, S., Zhao, M., Zhou, M., Li, Y.C., Wang, J., Gao, B., Sato, S., Feng, K., Yin, W., Igalavithana, A.D., Oleszczuk, P., Wang, X., Ok, Y.S., 2019b. Biochar-supported nZVI (nZVI/BC) for contaminant removal from soil and water: A critical review. J. Hazard. Mater. 373, 820–834.

Wang, T., Li, C.T., Zhao, L.K., Zhang, J.Y., Li, S.H., Zeng, G.M., 2017a. The catalytic performance and characterization of ZrO$_2$ support modification on CuO-CeO$_2$/TiO$_2$ catalyst for the simultaneous removal of Hg-0 and NO. Appl. Surf. Sci. 400, 227–237.

Wang, T., Liu, J., Zhang, Y., Zhang, H., Chen, W.Y., Norris, P., Pan, W.P., 2018b. Use of a non-thermal plasma technique to increase the number of chlorine active sites on biochar for improved mercury removal. Chem. Eng. J. 331, 536–544.

Wang, X., Wang, S., Pan, X., Gadd, G.M., 2019c. Heteroaggregation of soil particulate organic matter and biogenic selenium nanoparticles for remediation of elemental mercury contamination. Chemosphere 221, 486–492.

Wang, X., Zhang, D., Pan, X., Lee, D.J., Al-Misned, F.A., Mortuza, M.G., Gadd, G.M., 2017b. Aerobic and anaerobic biosynthesis of nano-selenium for remediation of mercury contaminated soil. Chemosphere 170, 266–273.

Wang, Y., O'Connor, D., Shen, Z., Lo, I.M.C., Tsang, D.C.W., Pehkonen, S., Pu, S., Hou, D., 2019d. Green synthesis of nanoparticles for the remediation of contaminated waters and soils: Constituents, synthesizing methods, and influencing factors. J. Clean. Prod. 226, 540–549.

Wang, Y.D., Greger, M., 2004. Clonal differences in mercury tolerance, accumulation, and distribution in willow. J. Environ. Qual. 33, 1779–1785.

Wang, Y.J., Liu, Y., Wu, Z.B., Mo, J.S., Cheng, B., 2010a. Experimental study on the absorption behaviors of gas phase bivalent mercury in Ca-based wet flue gas de-sulfurization slurry system. J. Hazard. Mater. 183, 902–907.

Wang, Y.J., Tian, Y., Zang, W.C., Jian, X.D., 2016c. Study on treatment and recycling of mercury from waste mercury catalysts in China. In: Li, J., Dong, F. (Eds.), Selected Proceedings of the Tenth International Conference on Waste Management and Technology. Elsevier Science Bv, Amsterdam.

Wang, Z.H., Jiang, S.D., Zhu, Y.Q., Zhou, J.S., Zhou, J.H., Li, Z.S., Cen, K.F., 2010b. Investigation on elemental mercury oxidation mechanism by non-thermal plasma treatment. Fuel Process. Technol. 91, 1395–1400.

WHO, 2011. Guidelines for Drinking-Water Quality. World Health Organization.

WHO, 2017. Ten chemicals of major health concern. World Health Organization.

Wu, H., Sun, J., Qi, D., Zhou, C., Yang, H., 2018a. Photocatalytic removal of elemental mercury from flue gas using multi-walled carbon nanotubes impregnated with titanium dioxide. Fuel 230, 218–225.

Wu, J., Li, C.E., Chen, X.T., Zhang, J., Zhao, L.L., Huang, T.F., Hu, T., Zhang, C., Ni, B., Zhou, X., Liang, P.K., Zhang, W.B., 2017a. Photocatalytic oxidation of gas-phase Hg-0 by carbon spheres supported visible-light-driven CuO-TiO$_2$. J. Ind. Eng. Chem. 46, 416–425.

Wu, Q.-R., Wang, S.-X., Wang, Y.-J., 2017b. Projections of atmospheric mercury emission trends in China's nonferrous metalsing industry. China Environ. Sci. (China) 37, 2401–2413.

Wu, Q.R., Wang, S.X., Yang, M., Su, H.T., Li, G.L., Tang, Y., Hao, J.M., 2018b. Mercury flows in large-scale gold production and implications for Hg pollution control. J. Environ. Sci. 68, 91–99.

Xiong, C., Li, Y., Wang, G., Fang, L., Zhou, S., Yao, C., Chen, Q., Zheng, X., Qi, D., Fu, Y., Zhu, Y., 2015. Selective removal of Hg(II) with polyacrylonitrile-2-amino-1,3,4-thiadiazole chelating resin: Batch and column study. Chem. Eng. J. 259, 257–265.

Xiong, Y.Y., Li, J.Q., Gong, L.L., Feng, X.F., Meng, L.N., Zhang, L., Meng, P.P., Luo, M.B., Luo, F., 2017. Using MOF-74 for Hg^{2+} removal from ultra-low concentration aqueous solution. J. Solid State Chem. 246, 16–22.

Xu, W., Adewuyi, Y.G., Liu, Y., Wang, Y., 2018. Removal of elemental mercury from flue gas using CuOx and CeO$_2$ modified rice straw chars enhanced by ultrasound. Fuel Process. Technol. 170, 21–31.

Xu, W., Pan, J., Fan, B., Liu, Y., 2019. Removal of gaseous elemental mercury using seaweed chars impregnated by NH$_4$Cl and NH$_4$Br. J. Clean. Prod. 216, 277–287.

Xun, Y., Feng, L., Li, Y., Dong, H., 2017. Mercury accumulation plant Cyrtomium mac-rophyllum and its potential for phytoremediation of mercury polluted sites. Chemosphere 189, 161–170.

Yami, T.L., Du, J.Y., Brunson, L.R., Chamberlain, J.F., Sabatini, D.A., Butler, E.C., 2015. Life cycle assessment of adsorbents for fluoride removal from drinking water in East Africa. Int. J. Life Cycle Assess. 20, 1277–1286.

Yang, J., Zhao, Y., Ma, S., Zhu, B., Zhang, J., Zheng, C., 2016. Mercury removal by magnetic biochar derived from simultaneous activation and magnetization of saw-dust. Environ. Sci. Technol. 50, 12040–12047.

Yang, J., Zhao, Y., Zhang, S., Liu, H., Chang, L., Ma, S., Zhang, J., Zheng, C., 2017a. Mercury removal from flue gas by magnetospheres present in fly ash: Role of iron species and modification by HF. Fuel Process. Technol. 167, 263–270.

Yang, J.P., Zhao, Y.C., Liang, S.F., Zhang, S.B., Ma, S.M., Li, H.L., Zhang, J.Y., Zheng, C.G., 2018a. Magnetic iron-manganese binary oxide supported on carbon nanofiber (Fe$_{3-x}$Mn$_x$O$_4$/CNF) for efficient removal of Hg-0 from coal combustion flue gas. Chem. Eng. J. 334, 216–224.

Yang, W., Hussain, A., Zhang, J., Liu, Y., 2018b. Removal of elemental mercury from flue gas using red mud impregnated by KBr and KI reagent. Chem. Eng. J. 341, 483–494.

Yang, W., Liu, Y., Wang, Q., Pan, J., 2017b. Removal of elemental mercury from flue gas using wheat straw chars modified by Mn-Ce mixed oxides with ultrasonic-assisted impregnation. Chem. Eng. J. 326, 169–181.

Yang, Y., Liu, J., Liu, F., Wang, Z., Miao, S., 2018c. Molecular-level insights into mercury removal mechanism by pyrite. J. Hazard. Mater. 344, 104–112.

Yang, Z., Li, H., Feng, S., Li, P., Liao, C., Liu, X., Zhao, J., Yang, J., Lee, P.H., Shih, K., 2018d. Multiform sulfur adsorption centers and copper-terminated active sites of nano-CuS for efficient elemental mercury capture from coal combustion flue gas. Langmuir 34, 8739–8749.

Yin, D., He, T., Zeng, L., Chen, J., 2016. Exploration of amendments and agronomic measures on the remediation of methylmercury-polluted rice in a mercury mining area. Water, Air, Soil Pollut. 227.

Yuan, Y., Xu, H.M., Liu, W., Chen, L.H., Quan, Z.W., Liu, P., Qu, Z., Yan, N.G., 2019. Morphology-controlled synthesis and sulfur modification of 3D hierarchical layered double hydroxides for gaseous elemental mercury removal. J. Colloid Interface Sci. 536, 431–439.

Zarei, S., Niad, M., Raanaei, H., 2018. The removal of mercury ion pollution by using Fe$_3$O$_4$-nanocellulose: Synthesis, characterizations and DFT studies. J. Hazard. Mater. 344, 258–273.

Zeng, H., Wang, L., Zhang, D., Yan, P., Nie, J., Sharma, V.K., Wang, C., 2019. Highly efficient and selective removal of mercury ions using hyperbranched poly-ethylenimine functionalized carboxymethyl chitosan composite adsorbent. Chem. Eng. J. 358, 253–263.

Zhang, A.C., Li, C.W., Xing, W.B., Song, J., Su, S., Xiang, J., 2018a. Photocatalytic activity and characterization of AgCl/Ag composite for Hg-0 removal under fluorescent light irradiation. Asia-Pac. J. Chem. Eng. 13, 11.

Zhang, A.C., Zhang, L.X., Chen, X.Z., Zhu, Q.F., Liu, Z.C., Xiang, J., 2017a. Photocatalytic oxidation removal of Hg-0 using ternary Ag/AgI-Ag$_2$CO$_3$ hybrids in wet scrubbing process under fluorescent light. Appl. Surf. Sci. 392, 1107–1116.

Zhang, J.Y., Li, C.T., Zhao, L.K., Wang, T., Li, S.H., Zeng, G.M., 2017b. A sol-gel Ti-Al-Ce-nanoparticle catalyst for simultaneous removal of NO and Hg-0 from simulated flue gas. Chem. Eng. J. 313, 1535–1547.

Zhang, L., Wu, S., Zhao, L., Lu, X., Pierce, E.M., Gu, B., 2019a. Mercury sorption and desorption on organo-mineral particulates as a source for microbial methylation. Environ. Sci. Technol. 53, 2426–2433.

Zhang, P., Pan, W.G., Guo, R.T., Zhu, X.B., Liu, J., Qin, L., She, X.L., 2019b. The Mo modified Ce/TiO2 catalyst for simultaneous Hg-0 oxidation and NO reduction. J. Energy Inst. 92, 1313–1328.

Zhang, Q., Liu, N., Cao, Y., Zhang, W., Wei, Y., Feng, L., Jiang, L., 2018b. A facile method to prepare dual-functional membrane for efficient oil removal and in situ reversible mercury ions adsorption from wastewater. Appl. Surf. Sci. 434, 57–62.

Zhang, S.B., Zhao, Y.C., Wang, Z.H., Zhang, J.Y., Wang, L.L., Zheng, C.G., 2017c. Integrated removal of NO and mercury from coal combustion flue gas using man-ganese oxides supported on TiO$_2$. J. Environ. Sci. 53, 141–150.

Zhang, X.N., Li, C.T., Zhao, L.K., Zhang, J., Zeng, G.M., Xie, Y.E., Yu, M.E., 2015. Simultaneous removal of elemental mercury and NO from flue gas by V$_2$O$_5$-CeO$_2$/TiO$_2$ catalysts. Appl. Surf. Sci. 347, 392–400.

Zhao, H.T., Fan, H., Yang, G., Lu, L., Zheng, C.G., Gao, X., Wu, T., 2018a. Integrated dynamic and steady state method and its application on the screening of MoS$_2$ na-nosheet-containing adsorbents for Hg-0 capture. Energy Fuels 32, 5338–5344.

Zhao, H.T., Yang, G., Gao, X., Pang, C.H., Kingman, S.W., Wu, T., 2016a. Hg-0 capture over CoMoS/γ-Al$_2$O$_3$ with MoS$_2$ nanosheets at low temperatures. Environ. Sci. Technol. 50, 1056–1064.

Zhao, L.K., Li, C.T., Li, S.H., Wang, Y., Zhang, J.Y., Wang, T., Zeng, G.M., 2016b. Simultaneous removal of elemental mercury and NO in simulated flue gas over V$_2$O$_5$/ZrO$_2$-CeO$_2$ catalyst. Appl. Catal. B-Environ. 198, 420–430.

Zhao, T., Yu, Z., Zhang, J., Qu, L., Li, P., 2018b. Low-thermal remediation of mercury-contaminated soil and cultivation of treated soil. Environ. Sci. Pollut. Res. 25, 24135–24142.

Zheng, S.M., Gu, B.H., Zhou, Q.X., Li, Y.C., 2013. Variations of mercury in the inflow and outflow of a constructed treatment wetland in south Florida, USA. Ecol. Eng. 61, 419–425.

Zhu, C., Duan, Y., Wu, C.Y., Zhou, Q., She, M., Yao, T., Zhang, J., 2016. Mercury removal and synergistic capture of SO$_2$/NO by ammonium halides modified rice husk char. Fuel 172, 160–169.

Zubair, M., Daud, M., McKay, G., Shehzad, F., Al-Harthi, M.A., 2017. Recent progress in layered double hydroxides (LDH)-containing hybrids as adsorbents for water re-mediation. Appl. Clay Sci. 143, 279–292.